



CFD modeling of the fluid-dynamics present in the charging process of a dual-fuel (diesel-NG/diesel-hydrogen) engine

Rafael Antonio Menaca Cabrera

Trabajo de grado presentado para optar al título de Ingeniero Mecánico

Asesor

Iván Darío Bedoya Caro, Doctor (PhD)

Universidad de Antioquia
Facultad de Ingeniería
Ingeniería Mecánica
Medellín, Antioquia, Colombia
2022

Cita	Menaca Cabrera, 2022 [1]
Referencia Estilo IEEE (2020)	[1] R. A. Menaca Cabrera, “CFD modeling of the fluid-dynamics present in the charging process of a dual-fuel (diesel-NG/diesel-hydrogen) engine”, Trabajo de grado profesional, Ingeniería Mecánica, Universidad de Antioquia, Medellín, Antioquia, Colombia, 2022.



Grupo de Investigación Ciencia y Tecnología del Gas y Uso Racional de la Energía (GASURE).



CENDOJ

Repositorio Institucional: <http://bibliotecadigital.udea.edu.co>

Universidad de Antioquia - www.udea.edu.co

Rector: John Jairo Arboleda Céspedes.

Decano: Jesús Francisco Vargas Bonilla.

Jefe departamento: Pedro León Simancas.

El contenido de esta obra corresponde al derecho de expresión de los autores y no compromete el pensamiento institucional de la Universidad de Antioquia ni desata su responsabilidad frente a terceros. Los autores asumen la responsabilidad por los derechos de autor y conexos.



University of Antioquia
Faculty of Engineering

Rafael Antonio Menaca Cabrera

Submitted for the degree of:
Mechanical Engineer

**CFD MODELING OF THE FLUID-DYNAMICS
PRESENT IN THE CHARGING PROCESS OF A
DUAL-FUEL (DIESEL-NG/DIESEL-HYDROGEN)
ENGINE**

Advisor: PhD. Iván Darío Bedoya Caro

Mechanical Engineering Department
Gas Science and Technology Group and Rational Use of Energy (GASURE)

2021

Acknowledgements

“Very little is needed to make a happy life; it is all within yourself in your way of thinking.”

-Marcus Aurelius.

This work made me happy. This work made me feel alive. The work that has been made in the present project was not a pressure task. It was only the consequence of working with the right people, at the right moment and with immense disposition. The right people I have met are in there because of the engineering faculty, the University of Antioquia and absolutely due to GASURE lab. The right moment is owed to my parents and my family for helping and supporting me emotionally and economically. They are in my life when I need them and when the things do not go correctly, they always remember to me my path and focus again my energy. The disposition that I have presented in my formation is due to the wise historical people that through lectures and books have taught and motivated me to concentrate my intellect in a bigger purpose and in a life full of meaning. Finally, I am completely grateful to the people I have met in the university and in my life in the last five years; all of them have contributed to my enhance and my growing as engineer and a person.

Contents

List of Tables	v
List of Figures	vii
1 Introduction	3
1.1 Cold flow simulations	4
1.2 Dual-fuel compression ignition engines	8
1.3 Turbulence	8
2 Objectives	11
2.1 General objective	11
2.2 Specific objectives	11
3 Associated theories	13
3.1 Modelling of turbulence	14
4 Modelling of engine	17
4.1 Geometry	17
4.2 Combustion chamber and ducts	17
4.3 Valves and valve lift profile	18
5 Numerical Approach	21
5.1 Decomposing geometry	21
5.2 Meshing	25
5.3 Grid Independence and uncertainties	27
5.4 Boundary conditions, turbulence models and general simulation settings	28
5.4.1 Boundary conditions	28
5.4.2 Turbulence model	31
5.4.3 Other settings	31
6 Results and analysis	33
6.1 Influence of turbulence models	33
6.1.1 Flow patterns	33
6.1.2 Velocity contours	35
6.1.3 Pressure contours and adverse pressure	36
6.2 Influence of substitution and enrichment level	39

6.2.1	Flow characteristics	39
6.2.2	In-cylinder air motion	43
Bibliography		49

List of Tables

3.1	Model constants for $k - \varepsilon$ turbulence models.	15
4.1	Properties, characteristics and operating conditions of the diesel engine.	17
5.1	Number of elements used in each mesh for the GI.	27
5.2	Fuel properties.	30

List of Figures

1.1	Final consumption of energy in Colombia in the year 2018 (a) and distribution of energetic matrix in the Colombian transport sector [6].	4
1.2	Velocity contour result of a cold flow simulation of the interaction between a diesel spray and the piston bowl in a diesel engine at the end of the compression stroke. Modified from [19].	6
1.3	Fuel distribution (mass) of Methanol injected in the intake duct of a dual-fuel diesel engine [15].	6
1.4	Schematic appreciation of the flow patterns (swirl and tumble) involved the in-cylinder air motion of an engine, with the respective axis and directions [31].	7
1.5	Representation of squish flow preceding to tumble flow in IC engines [27].	8
4.1	Information of the piston offered by catalogue [16].	18
4.2	Shape, proportions and critical design areas of typical inlet (a) and exhaust (b) valves and ports [22].	18
4.3	Valves lift profile and strokes distribution. 0 CAD corresponds to the TDC at the start of expansion stroke.	19
4.4	Final geometry constructed for the 4JH1-TC engine.	19
5.1	Flowchart for cold flow simulations of diesel engines [7].	22
5.2	Project Schematic in IC Engine of Workbench.	23
5.3	Decomposed diesel engine geometry at TDC.	23
5.4	Fluid zone names of decomposition for an engine with straight valves [3].	24
5.5	Mesh at TDC with the characteristics of fineMesh.	25
5.6	Skewness of mesh elements of mesh at TDC.	26
5.7	Aspect ratio of mesh elements of mesh at TDC.	26
5.8	Orthogonal quality of mesh elements of mesh at TDC.	26
5.9	GI in terms of SR (a) and TR (b).	28
5.10	The 3-node model for heat wall fluxes estimation [47].	29
6.1	Swirl ratio vs CAD for different turbulence models.	34
6.2	Tumble ratio vs CAD for different turbulence models.	35
6.3	Cross tumble ratio vs CAD for different turbulence models.	35
6.4	Velocity magnitude contours for different turbulence models at 460 CAD.	37
6.5	Pressure profile for different turbulence models at 345.5 CAD.	38

6.6	Zoom of gap between valve seat and intake valve appreciating adverse pressure at 345.5 CAD.	38
6.7	Swirl Ratio vs CAD for the difference substitution and enrichment levels.	39
6.8	Tumble Ratio vs CAD for the difference substitution and enrichment levels.	40
6.9	Cross Tumble Ratio vs CAD for the difference substitution and enrichment levels.	41
6.10	Velocity contours progression of the 100 air case.	42
6.11	TKE prior to diesel injection for different cases of enrichment and substitution (705 CAD).	43
6.12	Velocity contours at 660 CAD for different cases of enrichment and substitution (705 CAD).	44
6.13	Hydrogen mass fraction of 10 H ₂ case at TDC after compression stroke.	45
6.14	Velocity vectors in a 3D view in the middle stage of the intake stroke.	45
6.15	Flow patterns vectors perpendicular to the cylinder at 705 CAD (prior diesel injection) for different cases of enrichment and substitution.	46

Abstract

In this work was made a CFD cold flow simulation of a dual fuel diesel-natural gas (NG)/hydrogen engine. The simulation was made aimed to characterize and understand the flow behaviour in-cylinder and the effect of a dual gaseous fuel addition to the flow patterns and the main flow values that affect how combustion process is realized in the engine. Main flow patterns as swirl and tumble were analyzed with main fuel energy share (of NG and hydrogen) as parameter. The model was realised in Ansys Workbench as pre-processor and Ansys Fluent as solver. In order to set the model, it was made a general literature review to define the models and sub-models used in internal combustion engines cold flow simulations. Then, a recompilation of most important engine data (4JH1-TC) was executed. With the engine data, a 3D solid was constructed to feed the pre-processor. Consequently, the geometry was meshed in three different meshes with the aim of capture the grid independence. After grid independence, the model was fully established and the main simulations were carry out. Results show as a trend an increasing in the flow patterns when substitution/enrichment levels were increased. An hypothetical response to this influence is the physical properties of the hydrogen and NG, gases that are lighter than the air and with higher molecular diffusivity (hydrogen), thus having bigger disorder in the motion in-cylinder enhancing the flow movement intensity. In the meanwhile study, a parallel study was carried out aiming to select the best turbulence model for the type of simulation realized (cold flow simulation). Finally, some engineering applications for the model were presented, exploring fundamental aspects of internal combustion engines for the application of the model.

Resumen

En el presente trabajo fue realizada una simulación CFD de flujo frío de un motor de combustión dual diesel-gas natural (NG)/hidrógeno. La simulación fue realizada con la finalidad de caracterizar y entender el comportamiento del fluido al interior del cilindro y el efecto de la adición de combustible dual gaseoso sobre los patrones de flujo y los principales valores que afectan la forma en la cual se desarrolla la combustión en el motor. Principales patrones de flujo como el swirl y el tumble fueron analizados con el combustible gaseoso como parámetro (con base de contribución energética en porcentaje). El modelo fue desarrollado en Ansys Workbench como pre-procesador y Ansys Fluent como solver. Para setear el modelo, se hizo una general revisión de la literatura de estudios de cold flow haciendo uso del CFD en motores de combustión interna. Como paso siguiente, se realizó una recopilación de las características más importantes del motor (4JH1-TC) para ser modeladas en 3D como sólidos y alimentar el software con dicha información. Después de tener la geometría modelada, el proceso de mallado fue realizado, tomando tres mallas para la ejecución de la independencia del mallado. Al obtener la independencia del mallado, el modelo fue preparado para la realización de las simulaciones principales. Al analizar los resultados de cómputo, se encuentra una tendencia de crecimiento en los valores de los patrones de flujo a medida que el porcentaje de sustitución/enriquecimiento fue incrementado. Una hipotética respuesta a este comportamiento es la influencia de las propiedades termofísicas de los combustibles gaseosos, los cuales son más livianos que el aire y, en el caso del hidrógeno, más difusivo, provocando así movimientos más desordenados en el flujo aumentando la intensidad del movimiento del fluido al interior del cilindro. Al mismo tiempo en que las principales simulaciones se realizaban, un estudio

paralelo fue llevado a cabo para analizar el efecto del modelo de turbulencia sobre los resultados que se obtienen en simulaciones de flujo frío en motores de combustión interna. Finalmente, aplicaciones ingenieriles fueron mostradas con las cuales el modelo realizado puede ser aprovechado en futuros trabajos.

Chapter 1

Introduction

Carnot cycle lectures were an inspiration for Rudolf diesel. He was intrigued by low efficiencies achieved by the engines of his epoch. He proposed a task for himself: finding an engine with better characteristics, performance and efficiencies than the achieved by other known engines of his times [45]. Diesel engines are the most efficient engines available at the present time (although opposed piston engines are arising again with extremely high efficiencies [43]). These engines transport large quantities of products via sea and roads, provide power to a huge equipment all around the world, and, to complement, produce energy with the highest feasibility compared with similar apparatus [33]. Nevertheless, diesel engines have undesirable effects over environment because of their emissions. These contaminants are aiming to be reduced and new standards in the normative are being established. In order to mitigate the adverse effects of the engines, some researchers have collected the most significant advances in the reduction of pollution gases with different methodologies as re-circulation of exhaust gases, advanced technologies in diesel injection, diesel particle filters, etc [25, 26]. In a future proposal for the conservation of the diesel engine is suggested the necessity for introducing hydrogen as fuel in these devices [12]. The concept of dual-fuel engines with a main fuel cleaner than conventional hydrocarbon fuels (CH₄ or hydrogen) is gaining a strong traction [28]. As shown in Fig. 1.1, the biggest consumer in the Colombian energetic matrix is the transport sector.

In the presented context, a gap to analyze the effect of gaseous fuels going into the cylinder of the diesel engine mixed with air over the in-cylinder flow behavior is of special interest. With the expected reception of new dual-fuel engines technologies, it is important to analyze the repercussion of fuels introduced via intake ducts in gaseous state over the turbulence and in-cylinder flow behavior, due to the importance of the flow development over combustion process and overall engine work.

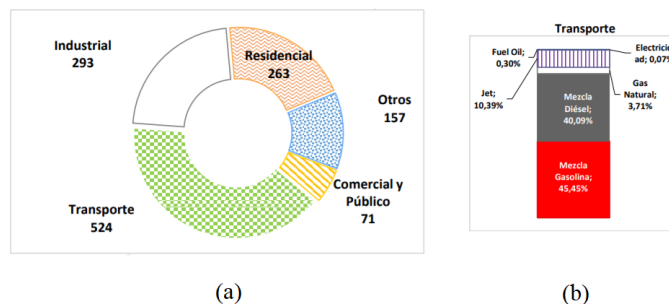


Figure 1.1: Final consumption of energy in Colombia in the year 2018 (a) and distribution of energetic matrix in the Colombian transport sector [6].

1.1 Cold flow simulations

Nowadays, the use of numerical models to simulate physical problems is almost mandatory for researchers and designers. Computational fluid dynamics (CFD) simulations allows an approach relatively fast and cheap to fluid-dynamic associated phenomena and engine performance parameters. CFD provides an appropriate approximation to systems where thermodynamics influences the fluid behavior [42]. The phenomena involved in internal combustion (IC) engines is extremely complex. The combustion in-cylinder, movements of the geometry and too short times where all these episodes occur contributes to the difficulty of the understanding of engines. Fortunately, due to the advances in computation and physical understanding, these events can be predicted via calculations and computations. CFD can be used to analyze the behavior of fluid flow without high expenses [7]. The value of results in CFD simulations on IC engines depends on the capability to capture the in-cylinder turbulence and flow patterns to represent the air-fuel air motion and the general behavior of the fluids [52].

The capacity to supply optimum flow conditions as high discharge coefficient, adequate swirl rate (SR) and tumble rate (TR), can result in an improvement of engine performance and a reduction in fuel consumption, polluting emissions and noise [44]. Additionally, the combustion is affected by these flow patterns. In that sense, it is possible to have a virtual control and stabilization of the combustion. The propagation of the flame depends on the flow patterns and the turbulence intensity. Thus, providing corrects in-cylinder air-fuel motions is recommended to enhance the combustion process. The flow patterns and how these are formed from admission ducts affect directly the engine performance and polluting emissions in diesel engines [35]. In [13] was found that high combustion efficiencies are controlled by high SR. However, in [10] is concluded that there is no a unique suitable SR value to satisfy all necessities in the engine operation. They argue that for each requirement in engine performance and polluting emissions, there is a value of optimum SR. In addition, high amount values in turbulent kinetic energy (TKE), SR and TR allow a better mixing of the charge and a faster combustion time and consequently a better combustion

efficiency [8, 48]. At this point, it is perceived the importance of flow patterns and turbulence and how it can affect significantly combustion efficiency, polluting emissions and also engine comfort. CFD simulations are needed to make these predictions in order to modify and design engines with best attributes that satisfy government requirements. Cold flow simulations are analysis of the airflow and possibly the fuel injection in IC engines. The simulation of an engine intrinsically report a transitory nature because of the moving, deforming and dynamic mesh. cold flow studies model the flow and its interactions in the process of an engine cycle without chemical reactions (non-reactive flow). The principal objectives of cold flow analysis are focused on 2 phenomena: 1. Capturing the mixture formation. 2. Accounting of SR, TR and in-cylinder turbulence. The cold flow studies identify and improve the in-cylinder fluid flow. Through cold flow simulations is possible to establish the basis of an optimum flow of fluid going into cylinder with high performance in terms of volumetric efficiency [35]. The dual-fuel engines with NG as main fuel have shown some decentralized behaviour of the ignition point [29, 50, 51]. It means that the maximum peak of pressure occurs far from the TDC in the compression stroke. Starting with cold flow simulations, it is possible to analyze the effect of main fuels as dual fuels (NG and hydrogen) in the flow patterns and the turbulence achieved in-cylinder. The turbulence could be reduced because of the thermophysical properties of the new gases allowed in the intake duct (not only air as occurs in conventional engines but also hydrogen and NG). These types of studies could offer a deep understand of the conduct of the fluid flow in the engine. The cold flow simulations have been studied by a lot of authors. All the focus are different in context but similar in goals. The cold flow simulations are aimed to provide the best in-cylinder fluid flow conditions. In fact, the flow patterns (swirl, tumble...) have been studied by many authors. In [10] was studied the effect of swirl in a heavy-duty diesel engine. The effect of swirl over combustion was tested. As exposed, the results showed a strong relation between swirl and combustion duration because of the turbulence intensity. As discussed before, the more turbulence, the faster combustion process. Additionally to experimental or numerical studies, some analysis have been realized in form of reviews about the influence of flow patterns and turbulence over engine efficiency, emissions and overall performance [23, 27]. To illustrate the cold flow simulations, some studies and simulation results are going to be presented. In the Fig. 1.2 is presented a cold flow simulation focused on the interaction of the spray with the combustion chamber.

The most similar study compared to the present research work was carried out in [15]. In that work was studied the influence of gaseous fuels in the overall fluid flow of a dual-fuel diesel engine. An important result of their work is presented in the Fig. 1.3.

In the Fig. 1.4 is presented the axis and directions definition of the swirl and tumble. The theoretical expressions to calculated the magnitudes of these variables are presented in the final of this section.

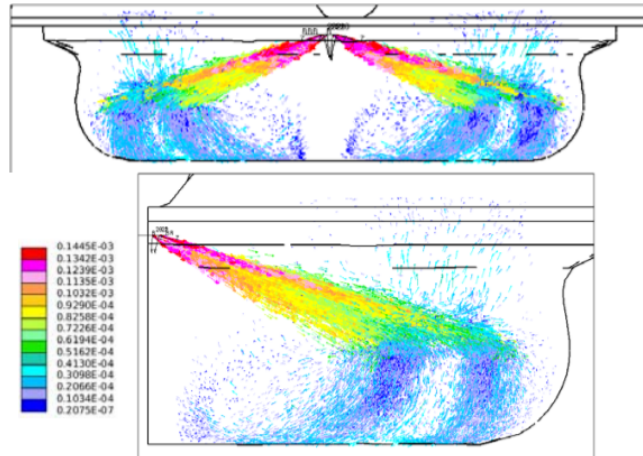


Figure 1.2: Velocity contour result of a cold flow simulation of the interaction between a diesel spray and the piston bowl in a diesel engine at the end of the compression stroke. Modified from [19].

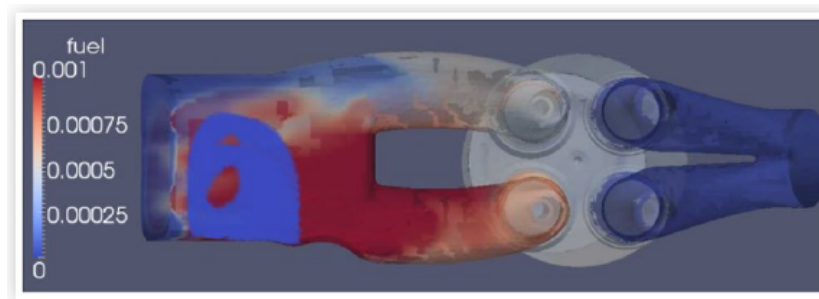


Figure 1.3: Fuel distribution (mass) of Methanol injected in the intake duct of a dual-fuel diesel engine [15].

Swirl

The flow motion around the cylinder axis is called swirl. The circular and descending motion of the in-cylinder flow is denominated as swirl. Swirl is one of the most dominant flow patterns that occur in-cylinder and this motion has a big impact over engine operation (combustion efficiency, emissions, performance) in the engine [13]. Swirl ratio is defined as follows [44]:

$$SR = \frac{\omega_s}{2\pi N} \quad (1.1)$$

where ω_s is the angular velocity of rotating flow at swirl axis and N is the speed of the engine. The IC engine program of Workbench deduces automatically this variable. The program uses the follows correlation:

$$SR = \frac{L_{sa}}{I_{sa}} \frac{2\pi N}{60} \quad (1.2)$$

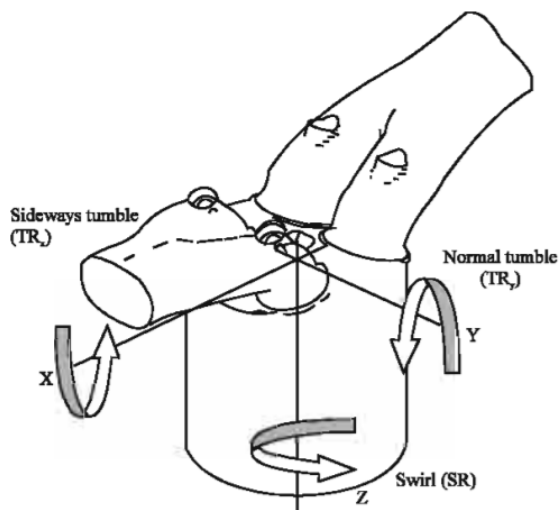


Figure 1.4: Schematic appreciation of the flow patterns (swirl and tumble) involved the in-cylinder air motion of an engine, with the respective axis and directions [31].

where L_{sa} is the magnitude of the angular momentum of the fluid with respect to the swirl axis, I_{sa} is the momentum of inertia of the fluid mass respect to swirl axis and N is the engine velocity in RPM.

Tumble

Tumble is another important flow pattern of the in-cylinder fluid motion. This pattern intensify the turbulence and could trigger a faster and more efficient combustion process. The tumble is quantified via TR. Tumble is defined as a rotational flow that takes place about a circumferential axis in the periphery of the piston bowl. In Ansys IC engine, the followed correlation is used to quantify this variable [44]:

$$TR = \frac{L_{ta}}{I_{ta}} \frac{2\pi N}{60} \quad (1.3)$$

where L_{ta} is the value of the angular momentum of the fluid with respect to the tumble axis, I_{ta} is the momentum of inertia of the fluid mass respect to tumble axis and N is the engine velocity in RPM. Finally, CT is also calculated by IC engine program of ANSYS. The CT ratio is computed in a perpendicular axis to the tumble axis, in the same way that TR is calculated.

Squish

Before TDC (bTDC) in the compression stroke, a radial flow movement is perceived. This movement of the air-fuel mixture (in the present scenario) is called squish. The squish ratio (SQ) is

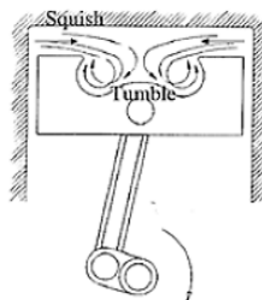


Figure 1.5: Representation of squish flow preceding to tumble flow in IC engines [27].

used in IC engines to quantify this flow phenomena. Squish precedes the tumble ratio. At the end of the compression stroke this organized movement is broken into small scale eddies promoting in-cylinder turbulence . An illustration of the squish is presented in Fig. 1.5.

In the present work the focus is established on swirl and tumble ratio and the squish is not analyzed deeply.

1.2 Dual-fuel compression ignition engines

Dual-fuel engines not only allow air in the intake duct, but also allow the primary fuel (if the main flow is of inducted type). The main fuel in dual-fuel engines can be used in three typologies [30]:

- Traditional engines (Otto and diesel) adding small quantities of gaseous fuel as additive, of the pilot fuel, via intake duct.
- External mixture of the gaseous fuel and a-posteriori forced ignition in the combustion chamber.
- Dual-fuel engine with direct or port injection of the main fuel.

In the present project, the dual-fuel diesel engine is going to be used as traditional engine with addition of small quantities of gaseous fuel (hydrogen and NG). This project is conducted in this way because of the necessary modifications that may be done to convert a diesel engine into a dual-fuel diesel engine (the typology used is such one with the minimum engine modifications).

1.3 Turbulence

The full power cycle of an diesel engine converted to HCCI was simulated by [21] in his master thesis. In the valve contours were found high velocities of the fluid in the first stage of the intake

stroke. Possible choked flow and counter-flow could appear affecting the volumetric efficiency. Adverse pressure could take place in that region promoting drastically a change in the charging process. When the intake valve is opened (IVO), the behavior explained above can appear. Additionally, it is established that some of the eddy viscosity models have weaknesses in certain problems. The presence of high curvature, swirl, separation, stagnation and body forces, promotes the failures in predictions made by those models [5]. In the present problem, a considerable change of area where the fluid flows (flow passing from intake valve to cylinder), is appreciated. Thus, the most common turbulence model used in literature to model turbulence in IC engines (Standard $k - \epsilon$), could present failures and throw misunderstanding results of some phenomena, specially in the first period after IVO event. Even, some works do not report turbulence models or global structure of simulation as the work made by [20]. It is supposed that the authors run the simulations in the configurations by defect (in terms of turbulence: Standard $k - \epsilon$ model). If a separating flow, a counter-flow or adverse pressure appears in first stage after IVO or some choking behaviour, the volumetric efficiency and the flow patterns could be severally affected. For this reason is recognized a gap for investigation to select the best turbulence models to reproduce flow patterns, flow, charging process and in-cylinder turbulence characteristics of an IC engine.

In order to obtain a more suitable understanding of the fluid behavior in the first stage of IVO, there were evaluated various turbulence models in the computation. It was made a cold flow simulation of a diesel engine focused in a portion of intake stroke (330.5 CAD to 460 CAD). In this portion of the engine cycle was analyzed the effect of changing the turbulence model over flow patterns and possibly choked flow found in the region around intake valve. In the present work the $k - \omega$ shear stress transport (SST) model was implemented. The $k - \omega$ SST model offers a superior results in terms of fluid separation because this model takes into account the transport of principal turbulent shear stress [38]. The $k - \omega$ SST turbulence model take advantage of the good predictions near walls of $k - \omega$ model and far from walls of $k - \epsilon$ model. In addition to $k - \omega$ SST turbulence model, Standard-, RNG- and Realizable $k - \epsilon$ turbulence models were performed. At last, Spalart-Allmaras turbulence model was executed in order to take advantage on attributes of this model referred to applications involving wall-bounded flows and boundary layers subjected to adverse pressure gradients (phenomena of interest of this work). The comparison between these models, conventional Standard $k - \epsilon$ model that can not offer answers about adverse pressures and those that can, will provide important information for future engine designs involving cold flow simulations in order to provide the best gas charging characteristics as discharge factor, turbulence intensity or in-cylinder flow patterns. This study tries to solve the concern of turbulence modeling for cold flow simulations in IC engines. In this investigation will be understood which turbulence model is the most practical model to execute cold flow simulations. In few words, the fact that the major cold flow studies are made simulating turbulence with $k - \epsilon$ as turbulence model, does not

mean that the model can predict correctly the in-cylinder turbulence phenomena. Hence, the above mentioned turbulence models were performed aiming to find the optimum turbulence model to use in cold flow simulations.

Chapter 2

Objectives

The objectives of the present final work are presented below:

2.1 General objective

The general objective of this final work is the realization of a cold flow CFD simulation of a dual fuel (NG-hydrogen) engine in the phase of charge (intake and compression stroke).

2.2 Specific objectives

- To realize a state of art review to establish models and sub-models used in CFD simulations in IC engines.
- To obtain a grid-independence in the realized simulation. Accordingly, it is necessary to consider operating engine conditions and the engine geometry.
- To analyse the fluid-dynamics present in the charging process of the IC engine varying gaseous fuel substitution and enrichment (NG-hydrogen) regarding to in-cylinder turbulence levels and swirl and tumble rates.

Chapter 3

Associated theories

In CFD simulations Navier-Stokes equations are solved. In the computational domain these equations are discretized along finite volume method. The computational domain is divided into small volume portions (control volumes)/cells. The resulting equations conform a equation system that is solved by numerical schemes. The numerical schemes used in certain problem depends on the flow field to solve [2]. To solve the flow field in IC engines, it is necessary have into account the effect of boundary movements (piston and valves) over behaviour of fluid. For a moving boundary system, the integral form of Navier-Stokes equations for a conservative tensorial property ϕ , defined by mass unit in a control volume V limited by a closed surface S is represented as follows [34].

$$\underbrace{\frac{d}{dt} \int_V \rho \phi dV}_{\text{Change rate of } \phi} + \underbrace{\oint_S d\mathbf{S} \cdot \rho \phi (\mathbf{u} - \mathbf{u}_b)}_{\text{Convective transport of } \phi} = \underbrace{- \oint_S d\mathbf{S} \cdot \rho \mathbf{q}_\phi}_{\text{Diffusive transport of } \phi} + \underbrace{\int_V S_\phi dV}_{\text{Production/destruction of } \phi} \quad (3.1)$$

where ρ is density, \mathbf{u} is flow velocity vector field, \mathbf{u}_b is boundary velocity and \mathbf{q}_ϕ y S_ϕ are the sources/sinks of the property ϕ in the surface and volume, respectively. The Governing equations of the flow field come off Eq.(3.1). In the differential form, mass, momentum and energy equations are written as below.

$$\frac{\delta \rho}{\delta t} + \nabla \cdot (\rho \mathbf{u}) = 0 \quad (3.2)$$

$$\frac{\delta \rho \mathbf{u}}{\delta t} + \nabla \cdot (\rho \mathbf{u} \mathbf{u}) = \rho \mathbf{g} + \nabla \cdot \boldsymbol{\sigma} \quad (3.3)$$

$$\frac{\delta \rho E_T}{\delta t} + \nabla \cdot (\rho \mathbf{u} E_T) = -\nabla \cdot \dot{\mathbf{q}} + \nabla \cdot (\boldsymbol{\sigma} \mathbf{u}) + \rho \sum_{k=1}^K Y_k \mathbf{F}_k (\mathbf{u} + \mathbf{V}_k) \quad (3.4)$$

In Eq.(3.3), only gravity is considered as body forces acting over particles in the fluid. More-

over, σ is the stresses tensor. According to Eq.(3.4), E_T is the total energy, $\dot{\mathbf{q}}$ is the volumetric rate of heat added by mass unity, Y_k is the mass fraction of k -specie present in fluid, \mathbf{F}_k is the volume forces acting over k -specie and V_k is the diffusion velocity of k -specie present in the fluid.

3.1 Modelling of turbulence

As stated in [49], when the turbulence (or variation of velocity respect mean quantities) in the Reynolds averaging procedure is taken into account, additional term in stresses tensor appears. A closure problem arises and it is necessary to obtain correlations in order to “close” the equations system. Boussinesq approximation is used in order to correlate the additional stress term with mean flow quantities. This approximation is observed in the Eq.(3.5).

$$-\rho \overline{u'v'} = 2\mu_t S_{ij}^* - \frac{2}{3}\rho k \delta_{ij} \quad (3.5)$$

where in left hand side appears the Reynold stresses term. In right hand side appears the correlation proportional to velocity, which is the rate of strain tensor in deviatoric form (S_{ij}^*), and a proportionality constant μ_t called turbulent viscosity. Boussinesq approximation is used in all the eddy viscosity models. The variation between models consists in how μ_t is calculated. The $k - \varepsilon$ (RNG, Standard and Realizable) turbulence models have two important factors: TKE k and turbulence dissipation rate ε . The transport equations of Standard $k - \varepsilon$ turbulence model are written as follows.

$$\frac{\delta}{\delta t}(\rho k) + \nabla \cdot (\rho \mathbf{u}k) = \nabla \cdot \left[\left(\mu + \frac{\mu_t}{\sigma_k} \right) \nabla k \right] + P_k + P_b - \rho \varepsilon + S_k \quad (3.6)$$

$$\frac{\delta}{\delta t}(\rho \varepsilon) + \nabla \cdot (\rho \mathbf{u}\varepsilon) = \nabla \cdot \left[\left(\mu + \frac{\mu_t}{\sigma_\varepsilon} \right) \nabla \varepsilon \right] + C_1 \frac{\varepsilon}{k} (P_k + C_3 P_b) - C_2 \rho \frac{\varepsilon^2}{k} + S_\varepsilon \quad (3.7)$$

where, P_k is the production due to mean velocity shear, P_b is the production due buoyancy, S_k and S_ε are user-defined sources. σ_k , σ_ε , C_1 , C_2 , C_3 and C_μ are coefficients of the model. Posterior of calculating k and ε , μ_t is computed as follows.

$$\mu_t = C_\mu \frac{\rho k^2}{\varepsilon} \quad (3.8)$$

The equations that represent RNG and Realizable $k - \varepsilon$ turbulence models are similar to those presented in Eq.(3.6) and Eq.(3.7). For further information about these equations and for extra information about the meaning of each term in equations, refer to [4].

In Eq.(3.9) and Eq.(3.10) is presented the SST $k - \omega$ turbulence model.

$$\frac{\delta}{\delta t}(\rho k) + \nabla \cdot (\rho \mathbf{u} k) = P_k - \beta^* \rho \omega k + \nabla \cdot [(\mu + \sigma_k \mu_t) \nabla k] \quad (3.9)$$

$$\frac{\delta}{\delta t}(\rho \omega) + \nabla \cdot (\rho \mathbf{u} \omega) = \frac{\gamma}{v_t} P_k - \beta \rho \omega^2 + \nabla \cdot [(\mu + \sigma_\omega \mu_t) \nabla \omega] + 2(1 - F_1) \frac{\rho \sigma_\omega \omega^2}{\omega} \nabla k : \nabla \omega \quad (3.10)$$

where β , β^* , $\sigma_{\omega 1}$, $\sigma_{\omega 2}$ and γ are constants and auxiliary functions. ω is the specific turbulence dissipation rate, v_t constitutes, F_1 is a blending function in order to switch the model. Following the calculation of k and ω , μ_t is evaluated as follows.

$$\mu_t = \frac{\rho k}{\omega} \quad (3.11)$$

and the eddy-viscosity with the blending function F_2 limit the viscosity near walls. F_2 is one for boundary layers and zero for free shear layers. Eddy-viscosity is expressed in the next equation.

$$v_t = \frac{a_1 k}{\max(a_1 \omega : \Omega F_2)} \quad (3.12)$$

where a_1 is a constant and Ω is the shear strain rate. For more information about this model, it can be revised the work made in [37] and [38].

The way in which turbulence is modelled through Spalart-Allmaras model is presented in the Eq.(3.13).

$$\frac{\delta \bar{v}}{\delta t} + \nabla \cdot (\mathbf{u} \bar{v}) = c_{b1} S \bar{v} + \frac{1}{\sigma} [\nabla \cdot (\mathbf{v} + \bar{\mathbf{v}}) \nabla \bar{v} + c_{b2} (\nabla \bar{v})^2] - c_{w1} f_w \left(\frac{\bar{v}}{d}\right)^2 \quad (3.13)$$

where \bar{v} is a new variable representing v_t but with some variations close to the walls. S is the shear rate tensor. d is the distance from the flied point to the nearest wall. f_w is a variable that stores some constants and contributes to the destruction of turbulence. σ , c_{b1} , c_{b2} , c_{w1} are constants of the model. Eddy-viscosity, for Spalart-Allmaras model, is computed as follows.

$$\mu_t = \rho \bar{v} f_{v1} \quad (3.14)$$

For more information about this model, refer to [46].

Table 3.1: Model constants for $k - \varepsilon$ turbulence models.

Turbulence Model \ Coefficients	$C_{1\varepsilon}$	$C_{2\varepsilon}$	C_μ	σ_k	σ_ε
Standard k- ε	1.44	1.92	0.09	1	1.3
Realizable k- ε	-	1.9	-	1	1.2
RNG k- ε	1.42	1.68	0.0845	-	-

Chapter 4

Modelling of engine

4.1 Geometry

The geometry is important for the simulation. The more of geometry information collected, the better results in the calculations [15]. Some characteristics of the geometry are the core of the simulation. The principal engine parameters are presented Table 4.1. The best way to gather engine information is via engine manuals and measurements in the engine. Both of them were used in the present work for the ISUZU 4JH1-TC engine.

Table 4.1: Properties, characteristics and operating conditions of the diesel engine.

Model	ISUZU 4JH1-TC		
No. of cylinders	4	Minimum valve lift (mm)	0.2
Bore x stroke (mm)	95.4 x 104.9	Intake system	Turbocharged
Crank radius (mm)	52.25	Cooling system	Water refrigerated
Connecting rod length (mm)	168	Speed (rpm)	2000
Valves per cylinder	2	Compression ratio	18.3
Intake Valve Opening (IVO)	335.5 CAD	Intake Valve Closure (IVC)	595.5 CAD
Exhaust Valve Opening (EVO)	126 CAD	Exhaust Valve Closure (EVC)	386 CAD

4.2 Combustion chamber and ducts

Combustion chamber and piston were measured and structured via catalogue [16] and correlations (volume displaced, stroke, etc.). The measures obtained in catalogue are shown in the Fig. 4.1.

The ducts were constructed as presented in the Fig. 4.2 where starting from valve head diameter (D) can be designed the majority of ducts and valves geometry.










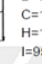



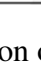





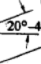

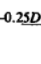
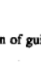







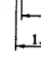
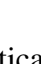








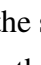
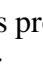
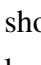
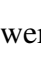
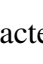




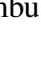
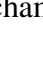










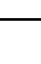
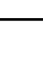
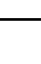



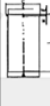
COMERCIAL DEL MOTOR		TARABUSI		AMT PARTS		PISTONES CAMISAS EQUIPOS		
								
								
								
								
								
								
								
								
								
								
								
								
								
								
								
								
								
								
								
								
								
								
		Diésel						ISUZU
Diésel-Motor 4JH1-TC 2999 cc.		95,4 4	49,9 -8,2 -20 88,9	31 x 76	1 2,5 1 2 1 3	 A=97 L=178,5 C=102,43 H=1,17 I=95,5 Cromada	REF. Nº P = PISTÓN 60-1053-000 C = CAMISA 40-0353 EC = EQUIPO	P.V.R. €
		Cámara Ø 45,2 mm. Inserto Galería de refrigeración Sin fresaduras válvulas						

Figure 4.1: Information of the piston offered by catalogue [16].

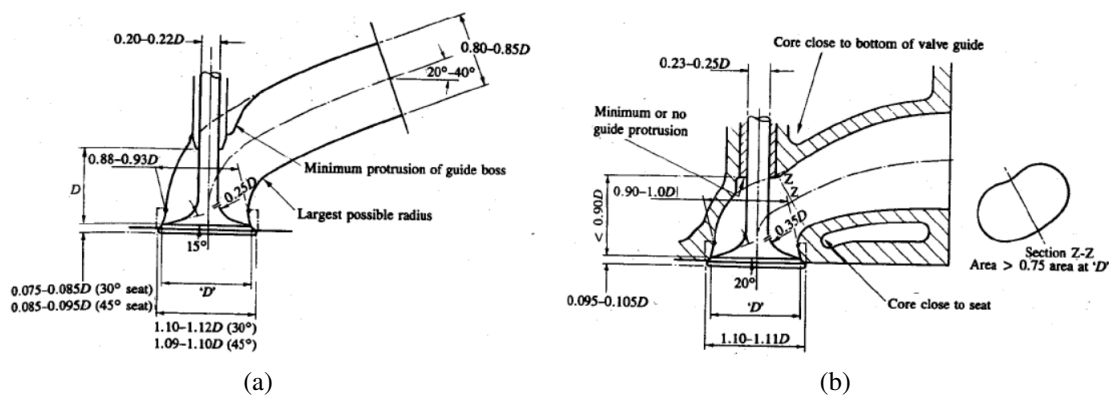


Figure 4.2: Shape, proportions and critical design areas of typical inlet (a) and exhaust (b) valves and ports [22].

4.3 Valves and valve lift profile

Furthermore, the valve lift profile and the strokes profile are shown in Fig. 4.3. The lift profile was constructed as suggested in [22], where the maximum lift valve is about 12% of the bore diameter. Additionally, from the engine manual were extracted the events (IVO, IVC, etc.) shown in Table 4.1.

The final geometry is presented in the Fig. 4.4. This geometry consist in intake and exhaust valves and ducts and a body of the combustion chamber.

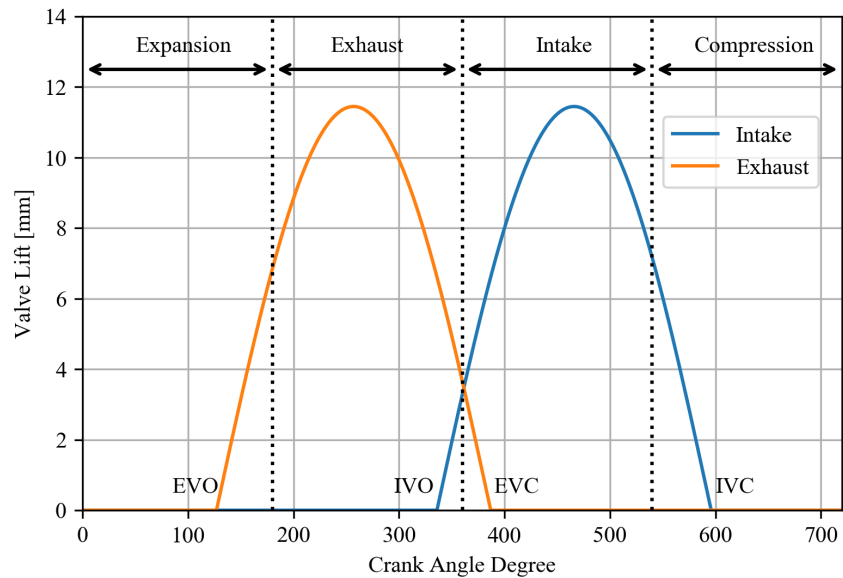


Figure 4.3: Valves lift profile and strokes distribution. 0 CAD corresponds to the TDC at the start of expansion stroke.

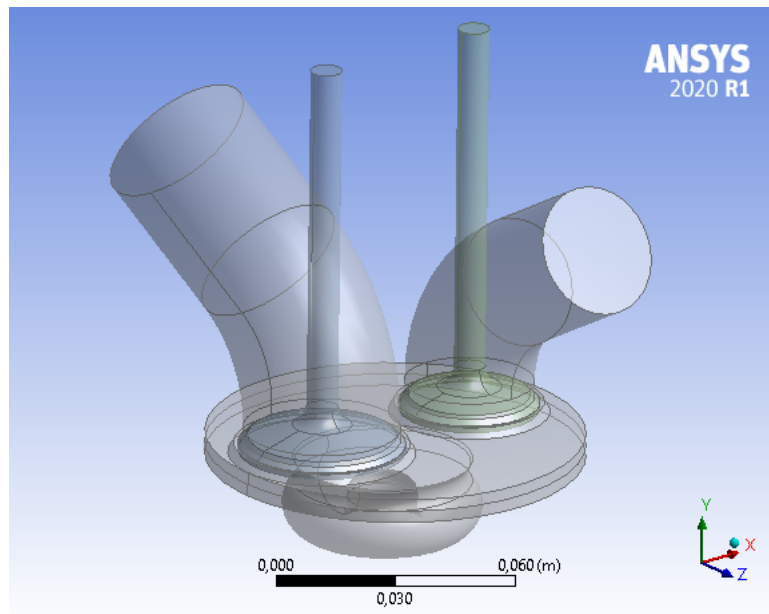


Figure 4.4: Final geometry constructed for the 4JH1-TC engine.

Chapter 5

Numerical Approach

There is a number of steps to be made in order to carry out a cold flow simulation. The main steps to do are organized in a flowchart realized in [7]. This flowchart is shown in the Fig. 5.1.

In fact, the step by step of the present cold flow simulation follows almost exactly the flowchart, but it was not known when the simulation was realized. In order to have a path to structure the presentation of the simulation made, this flowchart will be the scheme to understand what was made in each stage of this work. The first steps in the flowchart are solved in previous chapters. For example, objectives of the model are the objectives of the simulation. Collect available information and data for the model are the state of art revision and the consultation and creation of the geometry of the 4JH1-TC engine. Next step in flowchart shown in Fig. 5.1 is the specification of properties in ANSYS IC Engine. It is necessary to highlight that the simulations were run in the software ANSYS. ANSYS IC Engine of Workbench was used to structure the simulation and ANSYS Fluent was the solver of calculations. In that context, the first step in ANSYS IC Engine is to define the kind of simulation to realize in the tab ICE. In the present work, a cold flow simulation was selected. Furthermore, the software request valve lift profiles (Fig. 4.3) and some engine parameters. The project schematic of IC Engine in workbench is presented in Fig. 5.2.

5.1 Decomposing geometry

The next tab of the software solicits the engine geometry. Geometry has to be modelled in three main bodies: intake valve, exhaust valve and ducts with combustion chamber. These bodies feed the program (Workbench DesignModeler) in order to create the fluid region of the computational domain. Then, the geometry must be decomposed in order to have different geometry portions as recommended in the software guide [3]. This is made with the purpose of having a more suitable control of the computational domain. Each part and body in decomposed geometry is meshed with different specifications. The parts where the flow has greatest gradients (i.e. valves contours) have

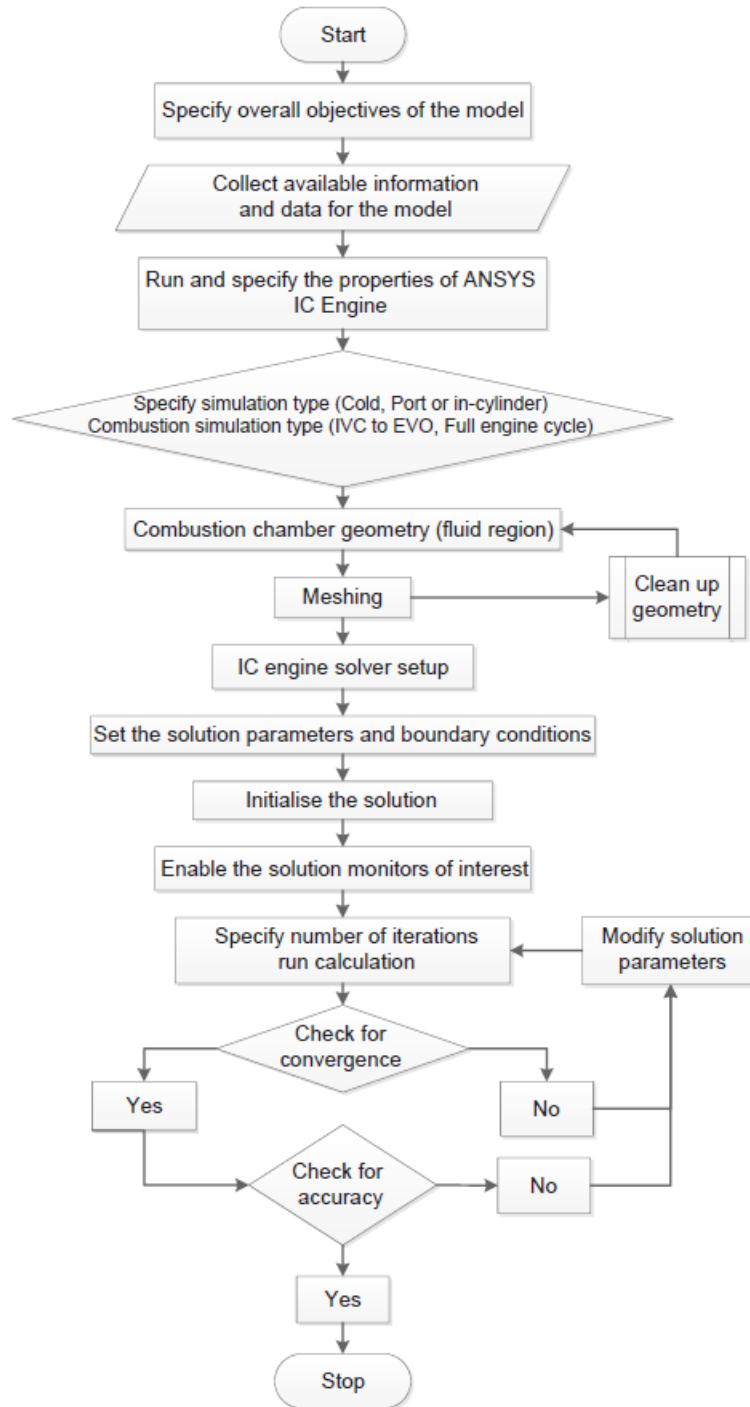


Figure 5.1: Flowchart for cold flow simulations of diesel engines [7].

the biggest element quantity. The decomposed geometry of the diesel engine is shown in the Fig. 5.3.

The decomposition is made into multiple fluid zones as shown in Fig. 5.4. These zones are as follows:

A	
1	IC Engine (Fluent)
2	ICE ✓
3	DM Geometry ✓
4	Mesh ✓
5	ICE Solver Setup ✓
6	Setup ✓
7	Solution ✓
8	Results ✓

4JH1-COLD-FLOW-SIMULATION

Figure 5.2: Project Schematic in IC Engine of Workbench.

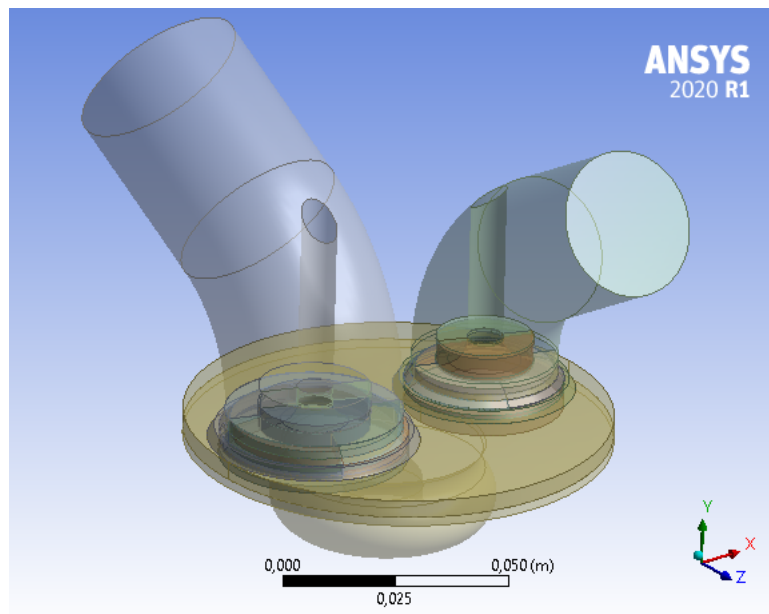


Figure 5.3: Decomposed diesel engine geometry at TDC.

- Zone 1: piston zone. This zone is fixed in all the simulation. The volume does not change. This zone represents the contour above piston shape.
- Zone 2: inferior combustion chamber. Fluid interaction with walls is important to take into account. This zone represents the transition between walls and cylinder. This volume changes in all the simulation because of the addition or elimination of elements in the different stages of simulation.

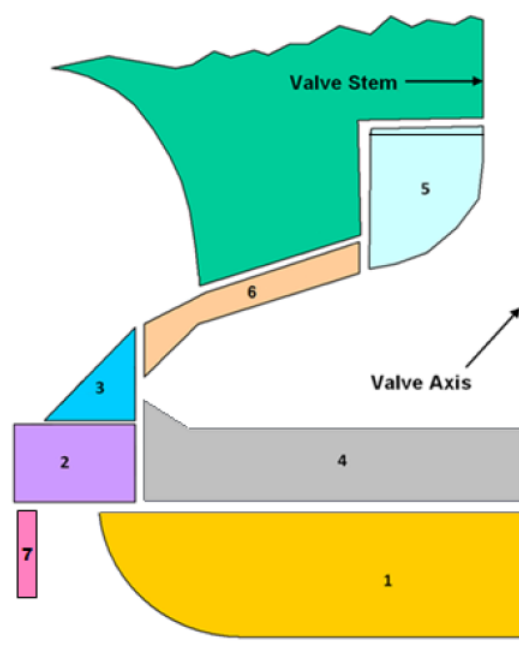


Figure 5.4: Fluid zone names of decomposition for an engine with straight valves [3].

- Zone 3: superior combustion chamber. In the moment of flow passing valves, there is a transition and this zone fulfills that function. Furthermore, when valves are closed, this zone is the boundary layer zone in the wall.
- Zone 4: cylinder zone below valve. This zone is the zone with major changes in all the power cycle. This zone is the combustion chamber and varies with the movement of the engine. This zone saves the in-cylinder flow patterns.
- Zone 5: rigid movement zone. This zone is above valves and does not change with in the cycle. This zone captures concavity of valves.
- Zone 6: layers of valves. This zone is one of the most important zones. In this region, the most dominant gradients are perceived. The flow patterns vary considerable because of the discharge of in-cylinder fluid and the small space to go through. This zone captures gradients around valves and change with the movement of valves.
- Zone 7: crevices zone. In this part, the fluid could go in leakage to crankcase. This zone was not taken into account in the simulation.

The piston movement is computed via engine parameters and rotation rate of engine (2000 RPM). With these parameters the IC engine program evaluate the profile of piston movement. The valve profile is taken from lift valve profile.

As shown in flowchart of Fig. 5.1, after geometry, it is necessary to establish the mesh.

5.2 Meshing

When the geometry is decomposed in Workbench DesignModeler, it is time to mesh the computational domain. The computational domain is divided into small elements with the aim of capturing the most precise gradients in the solution. The smaller the element, the better results in the calculation due to the catching of more information in each portion of computational domain. This is true until a certain quantity of elements where the number of elements does not influence the result. That is the reason of making a grid independence study. The grid independence study is made in Section 5.3. The mesh is made in Ansys Meshing. This program has a module of IC engines. In that module general characteristics of the mesh can be set. The mesh was made via this software and then smalls reparation in mesh were made in order to accomplish with the quality requirements of a mesh. The constructed mesh at TDC is shown in Fig. 5.5.

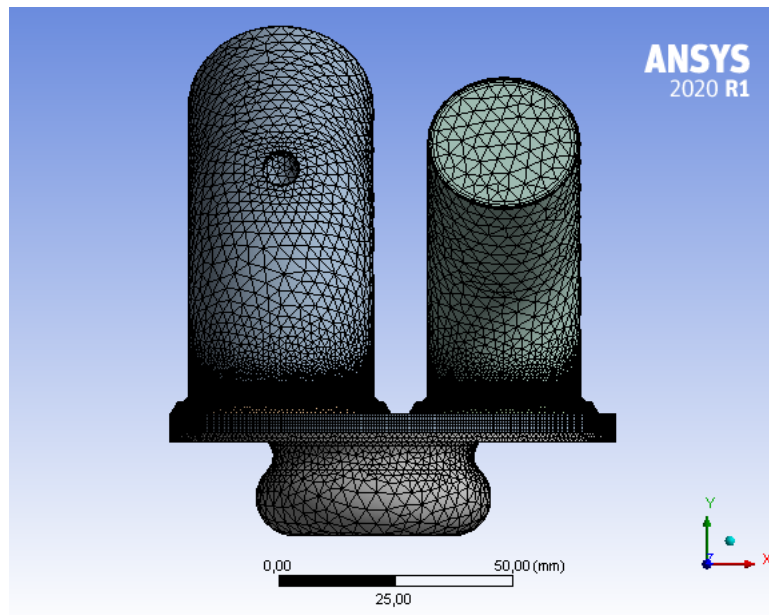


Figure 5.5: Mesh at TDC with the characteristics of fineMesh.

The mesh quality is verified via 3 mesh element metrics: skewness, aspect ratio and orthogonal quality and the results can be seen in Figs. 5.6, 5.7 and 5.8 respectively.

The majority of mesh elements accomplish with the mesh quality criteria. More than 95% of elements are far from bad mesh quality. In skewness, there are no elements in the bad quality mesh region. The elements with the biggest skewness represent those near valves where curves dominate the geometry. Orthogonal quality also presents a good performance with a high percentage

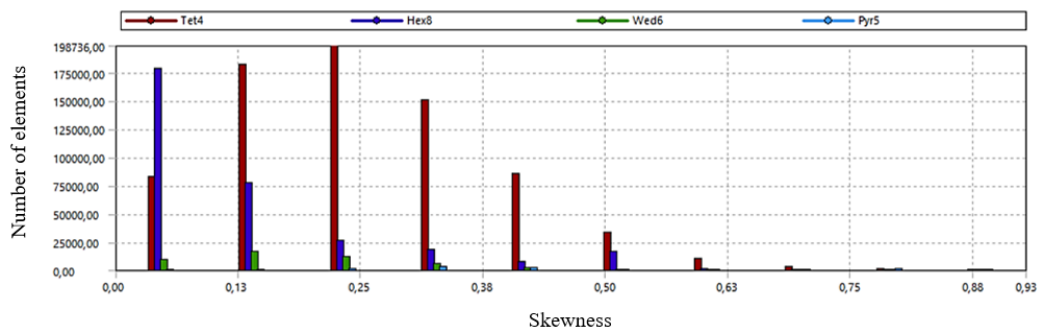


Figure 5.6: Skewness of mesh elements of mesh at TDC.

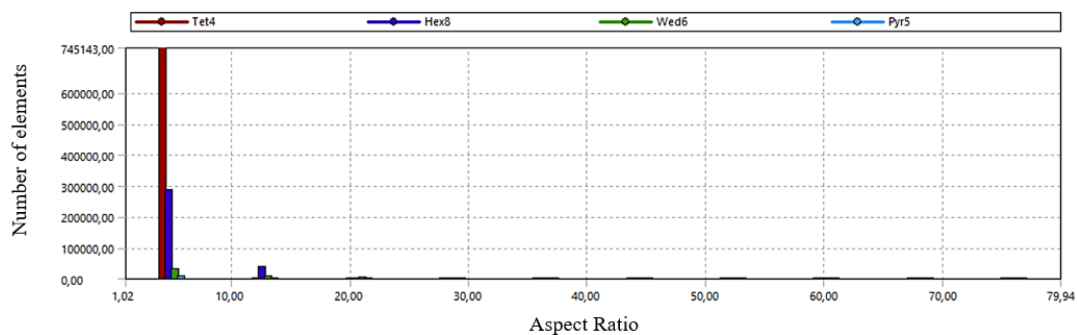


Figure 5.7: Aspect ratio of mesh elements of mesh at TDC.

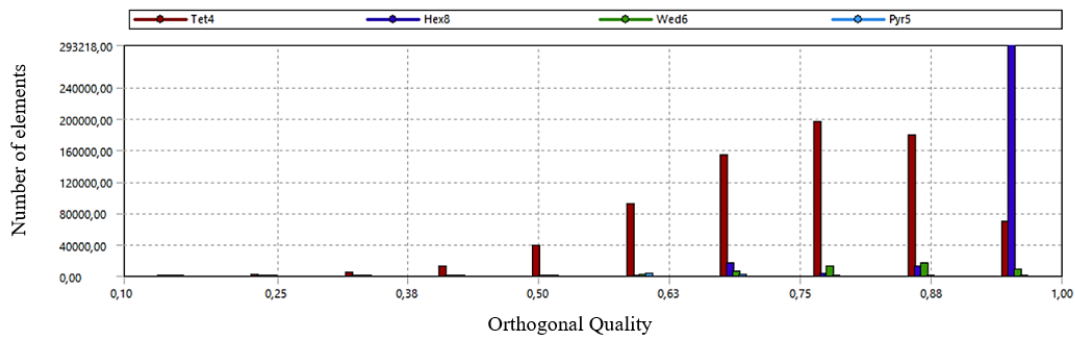


Figure 5.8: Orthogonal quality of mesh elements of mesh at TDC.

of elements with an adequate mesh quality. It is mandatory to remember that in the process of meshing, some problems can occur. In these situations, reparation in mesh is needed. As shown in flowchart, a clean up of geometry is essential. Sometimes curvatures are too aggressive and shall be smooth or sometimes engine characteristics in the geometry have to be deleted. Once an initial mesh accomplishing quality parameters is obtained, a requisite is to elaborate other meshes in order to study the grid independence.

5.3 Grid Independence and uncertainties

The Grid Independence (GI) is the process where the number of total elements of the mesh to run in the simulation is selected. This selection is made in terms of accuracy, convergence and simulation run time. The computational simulations collect some uncertainties and errors in its procedure (imprecise measures on geometries, mistakes in boundary conditions, etc.). That is why the *Journal of Fluids Engineering* published a ten element policy statement in order to bound and mitigate these problems with simulations [18]. In this policy is established that in all numerical simulations have to be carry out a GI. Some methods to calculate errors and uncertainties recommend three solutions. These solutions must be with different spacial resolution and each with the same refinement ratio [39]. This path was taken in the present simulation and the meshes used in the GI are shown in table 5.1. The refinement ratio was slightly conserved in the mediumMesh and fineMesh due to the complexity in the geometry.

Table 5.1: Number of elements used in each mesh for the GI.

Mesh	Air (%)	Number of elements (TDC)	Number of elements (BDC)
coarseMesh	100	564.827	1'257.211
mediumMesh	100	719.223	2'078.765
fineMesh	100	1'004.956	3'119.617

The simulations of the GI were focused in terms of SR and TR because of the importance of these flow patterns over combustion process. The result of the GI is shown in the Fig. 5.9 and a trend is appreciated in these results. All the results show a similar behaviour but differences in the magnitude value. The SR increases in intake stroke and it is kept in compression stroke. The SR increases in the last stage of the compression stroke. On one hand, in the SR, the maximum difference is about 17.5% between the results in coarse- and mediumMesh and fineMesh has average values between the other two results. On the other hand, in TR results, it is not possible to appreciate differences greater than 5% between all the calculations. In TR solutions, the behaviour is genuinely similar. There are some differences in the intake stroke but in compression stroke it is almost the same solution for coarse-, medium- and fineMesh. It is feasible to see that, in TR solution, fineMesh is smoother than the other calculations. Approximately, the variation between run time in the simulations is about one day in each simulation. The coarseMesh takes 48h in a 8 cores computer. In consequence, medium- and fineMesh take 3 and 4 days to simulate respectively.

Because of the smoothness in TR result, the average value in the calculations of the SR, and a reasonable run time, the fineMesh is selected to continue with the calculations.

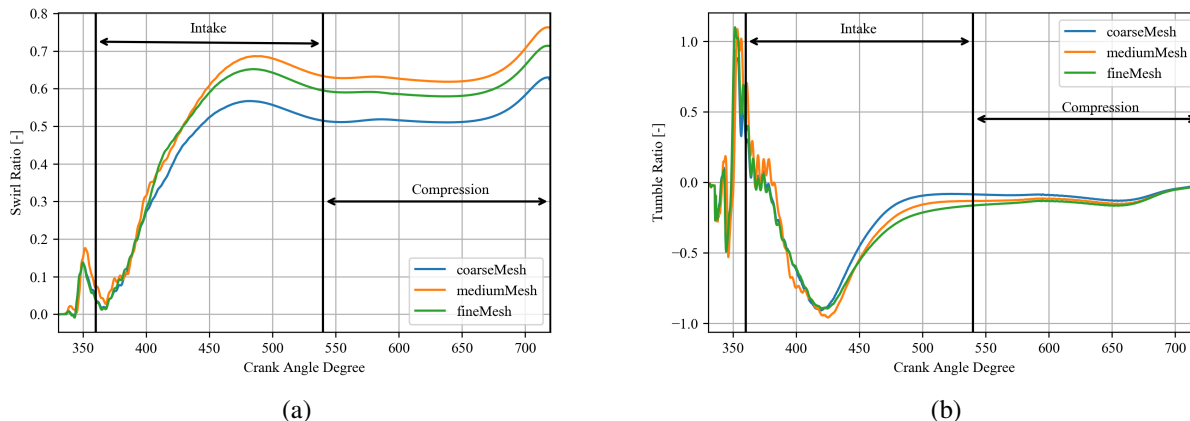


Figure 5.9: GI in terms of SR (a) and TR (b).

5.4 Boundary conditions, turbulence models and general simulation settings

As shown in the next tab to Mesh observed in Fig. 5.2, and in the flowchart of Fig. 5.1, when meshing is concluded, the time to set the simulation arrives. The IC engine of Workbench requests the RPM of simulation, the number of CAD to simulate, the frequency of saving and some other parameters.

5.4.1 Boundary conditions

In numerical simulations where partial differential equations are involved, artificial boundaries have to be established with the aim of limit the area of computation. Furthermore, boundary conditions are needed over these artificial boundaries in order to achieve good results in simulations [17]. In fact, to close the system of equations and to obtain acceptable results, boundary conditions must be prescribed to the artificial boundaries [11].

Walls

In IC engines heat transfer in walls is provoked because of gradients in temperature of in-cylinder fluid respect to coolant outside of cylinder or even oil of rings and crankcase. A concise study about wall temperatures in DI diesel engines was carry out [47]. In that study an engine A was tested in order to make the correlations to predict temperatures and heat fluxes through walls. With the result of engine A, the model was implemented in a engine B with similar specifications. These engines are too similar to the engine of this study. The model was adjusted and the results in engine

B were satisfactory. The model created to predict wall heat fluxes was acceptable. The 3 nodes model thermal circuit optimized in that work is presented in Fig. 5.10.

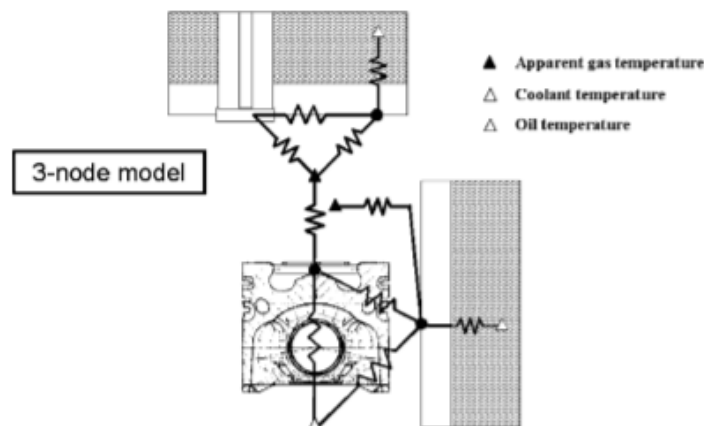


Figure 5.10: The 3-node model for heat wall fluxes estimation [47].

From that work were extracted the transfer heat coefficients for all fluids and these were set in the simulation. Some other works about engine cold flow simulations do not specify strictly the wall boundary conditions. For example, in [40] just is said that the correlation used can be found in a paper that uses Woschni model to calculate wall heat transfer fluxes. Another better information about boundary conditions in walls is offered in [36]. In this work an user defined function is constructed but it is not given or showed. In another work the wall temperatures just were initialized at 300K [7]. The last work also offers fixed walls temperatures with in-cylinder temperatures 200K bigger than inlet air temperature [41]. It should be important to establish the impact of some of these boundary conditions in the results obtained in the simulations.

Inlet and outlet

In conventional diesel engines, the fluid flow in intake ducts is only air. In the present work, the fluid entering to the cylinder is a mixture of air with NG and hydrogen. In fact, the parameters of the present work are the components of the mixture of the inlet gas flowing into cylinder via intake duct. In that way, the simulations realized in this investigation are the following cases:

- Case 10NG: Inlet mixture: 99,9947% Air + 0,0053% NG (mass) corresponding to 10% of contribution of NG in energy.
- Case 20NG: Inlet mixture: 99,9894% Air + 0,01061 % NG (mass) corresponding to 20% of contribution of NG in energy.

- Case 10H2: Inlet mixture: 99,998% Air + 0,002% H_2 (mass) corresponding to 10% of contribution of hydrogen in energy.
- Case 20H2: Inlet mixture: 99,996% Air + 0,004% H_2 (mass) corresponding to 20% of contribution of hydrogen in energy.
- Case 100 air: Inlet mixture: only air.

In Ansys Fluent the mixture is created when species transport is on. The mixture is created and then, the mixture in different boundaries has to be indicated. From [14] and [9] were extracted the properties of fuels. These properties can be seen in Table 5.2.

Table 5.2: Fuel properties.

Property	Diesel	Guajira NG	Hydrogen	Palm oil biodiesel
Low heating value (MJ/kg)	43	48.77	120	39.55
Simplified chemical composition	$C_{10.8}H_{18.7}$	97.76% CH_4 ;0.38% C_2H_6 ; 0.2% C_3H_8 ;1.29% N_2 ;0.37% CO_2 (by volume)	H_2	$C_{19.7}H_{36.9}O_2$
Stoichiometric air-fuel ratio	14.32	-	-	12.55

Furthermore, the fuel substitution level (Z) is expressed in the equation

$$Z = \frac{\dot{m}_D - \dot{m}_P}{\dot{m}_D} \quad (5.1)$$

where \dot{m}_D is the diesel mass flow rate and \dot{m}_P is the pilot mass flow rate. The balance to calculate flow mass rate of diesel and pilot fuels (NG and hydrogen) was made as follows. It was known an operation point of the diesel engine. That point operates in 2000RPM and the engine control unit receive a measure of diesel injected in that cycle. Thus, with the diesel mass flow rate and the LHV of the diesel, it is possible to compute the power offered by that diesel quantity. Then, that power should be equal to the energy offered by the new diesel quantity plus the energy supplied by pilot fuel, as shown in next relation.

$$Power = LHV_D Diesel_{Injected} = \dot{m}_D LHV_D + \dot{m}_P LHV_P \quad (5.2)$$

When Z is given by user, a 2x2 equation system can be solved. In that way was calculated the flow mass rate of fuels get into cylinder. As pilot fuels enter cylinder in gaseous state, it should be a new relation in order to obtain a mass fraction in ducts to set the boundary condition. Air mass flow rate also is offered by engine unit system. These parameters can be seen in the workshop engine manual of the 4JH1-TC engine. With the air mass flow rate and the pilot mass flow rate, the mass fraction can be composed with the aim of set the mixture entering cylinder. With the mass fraction of fuels, the inlet boundary condition was set. The temperature of inlet air and fuels is set to 298K. The pressure of that mixture in inlet is set to 2x site pressure (Medellín). This value was

found after of reading a lot of forums talking about the influence of turbocharger in the pressure of inlet charging. The outlet was set at site pressure of Medellín (84kPa).

5.4.2 Turbulence model

The form in which Reynolds stress are approximated via turbulence models has to be laid. In ANSYS Fluent turbulence model is put. Some works have worked with Standard $k - \epsilon$ turbulence model [7, 15, 31, 40, 41, 44, 53]. The majority of the works presented before are works about cold flow simulations in engines. Furthermore, the focus of these investigations was to analyze main in-cylinder characteristics of flow patterns, turbulence and interactions of fluid in the cylinder. In consequence, for cold flow simulations in IC engines, Standard $k - \epsilon$ turbulence model is well established and its results for these kind of problems show feasible congruence.

Here a dude arises: there are a lot of turbulence models with similar computational weight (2-equation turbulence models), but, why Standard $k - \epsilon$? This question was structured and, in results, some answers will be given with an article made because of this problem.

Finally, the $k - \epsilon$ turbulence model was used because of the popularity of this model in similar simulations.

5.4.3 Other settings

The run time simulation was set as 389.5 CAD, from 330.5 CAD (5 CAD before IVO) until 720 CAD (final stage of compression stroke). The simulation began in 330.5 CAD because of the recommendation of initialization 5 CAD before the case of study (initializing from the start of intake stroke). The time step was set in 0.25 CAD in normal conditions and 0.125 CAD five CAD before and after of an event in the cycle (i.e. IVO, EVO, etc.). Residuals were set in 1×10^{-6} for TKE. For energy and momentum equations 1×10^{-4} ; for continuity equation and species 1×10^{-3} . PISO scheme is used across Green-Gauss Node based for gradient and PRESTO! for pressure-velocity coupling. Second order upwind was set for discretization schemes of all equations.

Chapter 6

Results and analysis

Due the type of simulations (cold flow simulations) realized in this research, the focus of the results are those involving in-cylinder flow patterns and flow characteristics. In that sense, the principal flow characteristics are analyzed.

6.1 Influence of turbulence models

In order to evaluate the effect of the different turbulence models over the in-cylinder flow characteristics, various turbulence models were evaluated in a simulation of the intake stroke. The results of this analysis is structured below.

6.1.1 Flow patterns

The main flow patterns observed in IC engines are swirl, tumble and cross tumble (CT). The swirl ratio values for all models computed can be observed in the Fig. 6.1. It is noticed that the results for all turbulence models have a similar behaviour in the entire intake stroke. The results for SR are practically exact from 330.5 CAD to 337 CAD. In the first stage of the intake stroke (near 360 CAD), there can be seen some variations in the SR value for all turbulence models, although these variations tend to reduce when the intake stroke advances. The only model with considerable difference is, in fact, the Standard $k - \varepsilon$, that follows the same patterns than other models, but with a wide difference in the value. The results for others turbulence models are close between them as intake stroke progress. The results calculated for SR with Spalart-Allmaras and SST $k - \omega$ turbulence models suffer the least perturbations in the whole simulation. Spalart-Allmaras result shows an average tendency in the calculation and is close to the results obtained by rest of models. It can be considered Spalart-Allmaras turbulence model for SR as the most suitable because this model is a one-equation model, compared with all other models that are two-equation models. In

consequence, Spalart-Allmaras turbulence model is the cheapest model in terms of computational time.

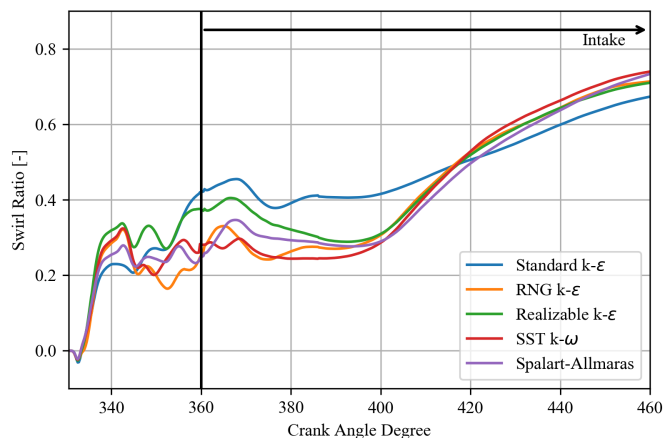


Figure 6.1: Swirl ratio vs CAD for different turbulence models.

TR is calculated with respect to x-axis and the results are shown in Fig. 6.2. From 330.5 CAD to 360 CAD the solution values of TR for all turbulence models are close with small fluctuations. In the first stage of intake stroke (near 360 CAD) it can be perceived a separation in the results of Standard $k - \epsilon$ model respect to other results. This separation is maintained in the rest of simulation becoming more significant after 400 CAD. As the results of SR simulations, the models have similar behavior for TR excluding the result for $k - \epsilon$ model that has a difference of almost 33% regarding to other turbulence models in 430 CAD. From the same point of view for SR results, the Spalart-Allmaras turbulence model is an appropriate model to calculate TR. Spalart-Allmaras turbulence model compared to other studied turbulence models has advantage in terms of computational time because of the less equations to solve, and because of the good achievement in results near to the rest of results.

The results of calculations for cross tumble ratio are shown in Fig. 6.3. These results have similar behavior as obtained for swirl and tumble ratios. For CT ratio simulations, it can be observed fluctuations between computed results of every turbulence models. In all the simulation (330.5 CAD to 460 CAD), the values obtained differ between them. The biggest difference can be observed near 430 CAD where it exists a difference of approximately 50% in RNG- and Realizable $k - \epsilon$ calculations respect to Standard $k - \epsilon$ model. SST $k - \omega$ and Spalart-Allmaras models have mean values between RNG with Realizable $k - \epsilon$ and Standard $k - \epsilon$. In the same manner than for SR and TR, the Spalart-Allmaras result for CT ratio has an outcome in the middle of the further turbulence models. Finally can be stipulated that, for cold flow simulations focused on flow patterns, the most advisable turbulence model is Spalart-Allmaras. Spalart-Allmaras model

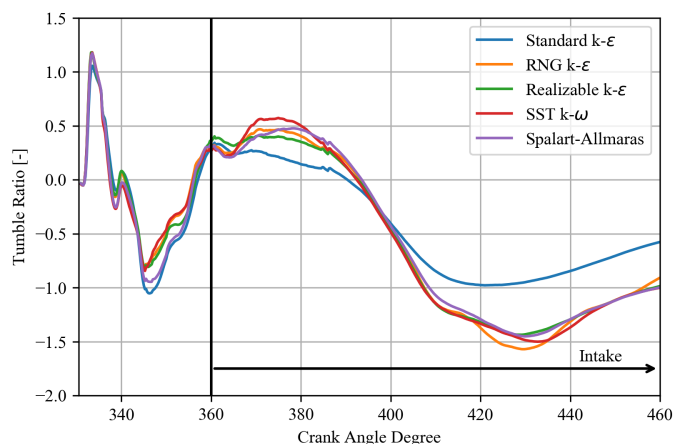


Figure 6.2: Tumble ratio vs CAD for different turbulence models.

has a similar behaviour in the results of all flow patterns. Furthermore, this model shows smooth results with less fluctuations compared to other models. In terms of computational time Spalart-Allmaras model has advantages because it solves one equations to model the turbulence and the rest of turbulence models solve 2 equations. In these kind of simulations where the simulations are too expensive in computational terms, Spalart-Allmaras model accomplish with the needs to obtain acceptable results.

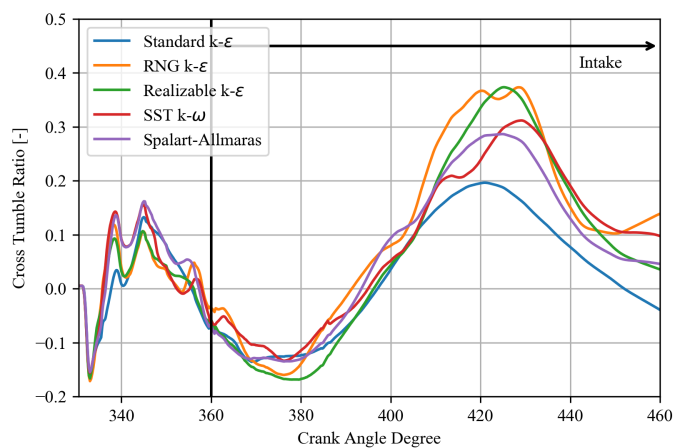


Figure 6.3: Cross tumble ratio vs CAD for different turbulence models.

6.1.2 Velocity contours

Fig. 6.4. illustrates the in-cylinder velocity profile for different turbulence models at 460 CAD (near max valve lift). The maximum velocities reached after passing intake valve are similar with

values around 80 m/s. The contours computed for all the models vary significantly between them. The wake formed by the fluid entering cylinder have different shapes in all turbulence models. The RNG model predicted a messy velocity profile compared to other models. The models $k - \epsilon$ Standard and Realizable and the Spalart-Allmaras model are similar between them showing organized and smoothed forms. It is perceived in SST $k - \omega$ and RNG $k - \epsilon$ models a peak of velocity above intake valve in the detachment region when fluid goes into cylinder. The wake of Standard $k - \epsilon$ model is the widest, but the other models have a deeper wake with bigger velocities (yellow/green thin wake). This fact suggest a more organized velocity profile in Standard $k - \epsilon$ model. Comparing Standard $k - \epsilon$ model (the most used model in literature), with the cheapest model regarding to computational time (Spalart-Allmaras), some similitude can be reported. The wake is analogous and the rest of the profile is comparable between these models. This suggest a validation to implement Spalart-Allmaras model in order to obtain a smaller computational time in simulations and finally obtaining related results to Standard $k - \epsilon$ model with feasible characteristics.

6.1.3 Pressure contours and adverse pressure

Fig. 6.5. represents the in-cylinder pressure contour at 345.5 CAD for different turbulence models. The general results show similitude between the turbulence models. There can be appreciated that all calculations except Standard $k - \epsilon$ have a gradient above intake valve with a circular form (orange color). This gradient is a vortex formed when IVO event begins. It can be noted that Standard $k - \epsilon$ model can not predict the mentioned vortex behavior. From the figure can be appreciated that the major gradient is captured by SST Standard $k - \omega$ model. It was expected this result because that model has a better approach to gradients near walls. In this study, it was important to analyze the pressure gradients in the first stage of IVO event, when could appear flow detachment, choked-flow or adverse pressure around intake valve region. The fundamental argument was that Standard $k - \epsilon$ could not offer such a outlook to predict correctly possible flow detachment or adverse pressure in the first stage of IVO event. It is important to observe that Standard $k - \epsilon$ results provide only mean values of the variables while, for example, SST $k - \omega$ tend to model those gradients in a more detailed way. For the rest of the contour, specially far from walls, pressure profiles do not differ significantly.

In the gap formed between valve seat and the intake valve when the valve starts to descend (see Fig. 6.6), another pressure gradient can be observed forming a shape of adverse pressure. It was expected a detachment of flow in this stage of the engine charge because of the physical conditions present in that time portion. Some gradients are perceived in the gap. This kind of gradients could trigger counter-flow (i.e. flow going into the intake duct) impeding a normal charging of air of the engine. As can be seen in Fig. 6.6, a blue portion (low pressure) near wall of the valve seat

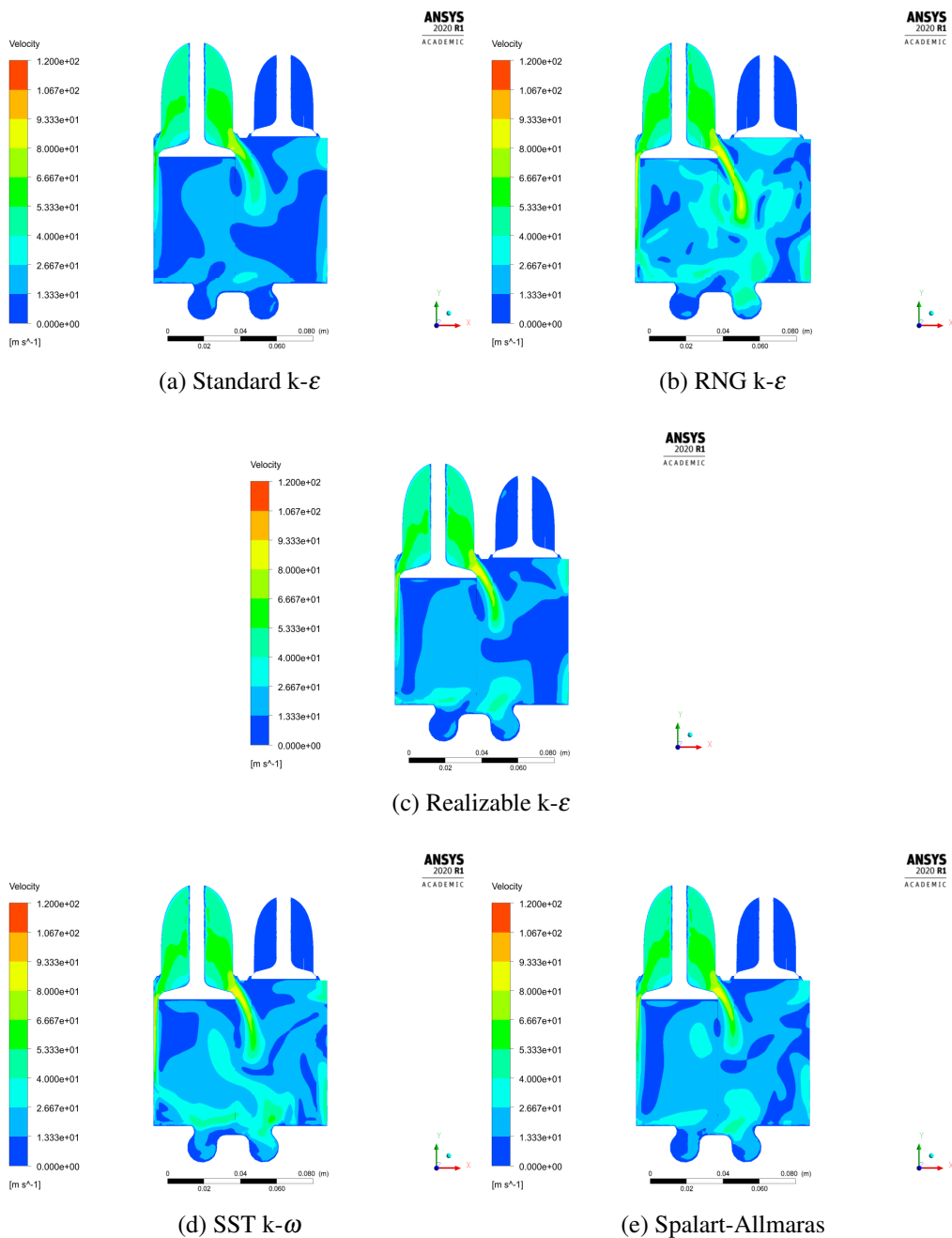


Figure 6.4: Velocity magnitude contours for different turbulence models at 460 CAD.

is found. In that region of low pressure, a counter-flow could take place. With this phenomena, a lower volumetric efficiency is expected. The back-flow acts as an obstacle impeding the correct entry of the charge into cylinder. As supposed, Standard $k - \epsilon$ model has an inferior prediction of this gradient compared to the other models of this study.

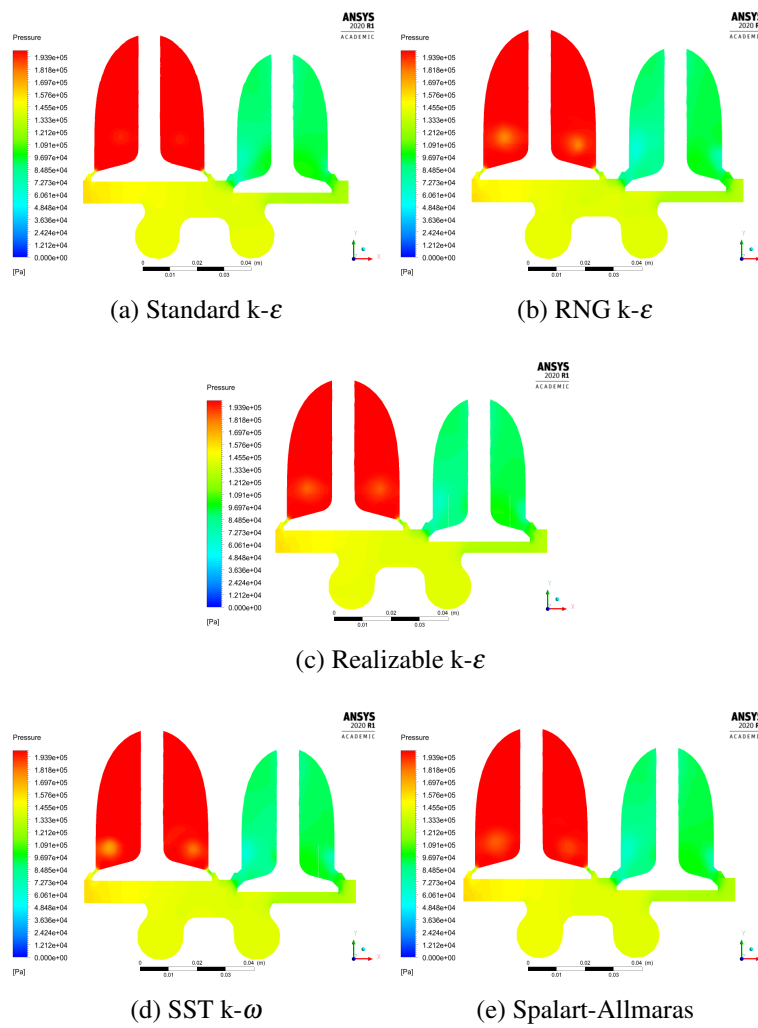


Figure 6.5: Pressure profile for different turbulence models at 345.5 CAD.

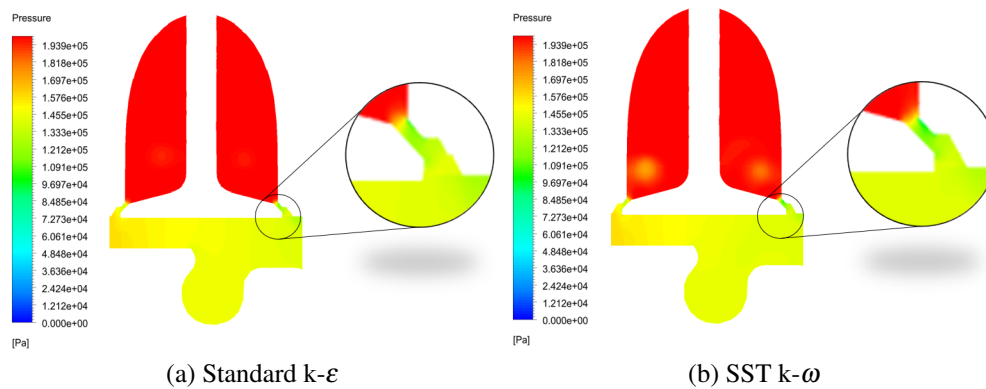


Figure 6.6: Zoom of gap between valve seat and intake valve appreciating adverse pressure at 345.5 CAD.

6.2 Influence of substitution and enrichment level

6.2.1 Flow characteristics

The principal flow patterns in cylinders are: swirl, tumble and cross tumble. These flow patterns were analyzed one by one. In first place, the SR was plotted for all the simulation cases (see Fig. 6.7). The first view of the graph offers a fact: the SR for the air is the smaller obtained compared to other cases. In the first stage of the intake stroke (near 360 CAD) the SR for the air is considerably smaller than the values computed for the other simulations. This behaviour suggests that the tangential velocity when the air-fuel mixture goes into cylinder is bigger than in the only air case. Near 360 CAD (TDC after exhaust stroke) a value of approximately 0 is computed for SR of the air, whereas for the rest of computed cases, the values are around of 0.45. In compression stroke the got values for the computations are close between them with variations smaller than 10 % and these reduce along the stroke. The biggest SR is obtained in the 10NG and 20H2 cases. The hydrogen and the NG are lighter than air, thus, the motion of the particles are more disordered, contributing to flow patterns more pronounced, with bigger gradients, provoking a bigger presence of turbulence in-cylinder.

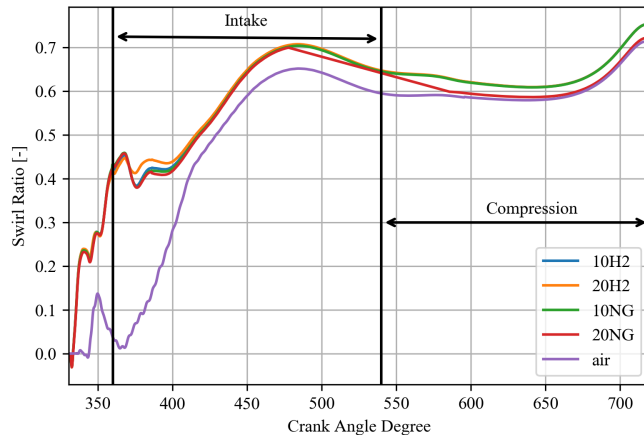


Figure 6.7: Swirl Ratio vs CAD for the difference substitution and enrichment levels.

A similar behavior to the SR can be seen in the TR results shown in Fig. 6.8. It is possible to appreciate a smaller TR in almost all the range of the simulation (intake and compression stroke). After BDC, when compression stroke begins, the trend of all the simulations is close, where the values converge in the final of the compression stroke (near 720 CAD) to an approximately value of zero because of the crunching produced by the piston arising TDC. The values of TR obtained for the cases with addition of gaseous fuel (10, 20 NG and H2) are indistinguishable. As the fact commented in the SR solution, a probable respond to this behave can be attributed to the physical

properties of the extra gases in the dual-fuel mode (hydrogen and NG lighter than air). TR in SOI (approximately 15 CAD bTDC in the compression stroke) is slightly bigger (as absolute value) for the dual-fuel mode cases than the value obtained for the 100 air case. This behavior is similar in the Fig. 6.7 for the SR with less difference. Because of the direct relation between TR (and SR with less impact) with the in-cylinder turbulence, it is expected a faster combustion for the dual-fuel mode operation. Furthermore, a small enhance in the efficiency could appear due to the expected increasing in the mixture quality and the reduction of the combustion duration.

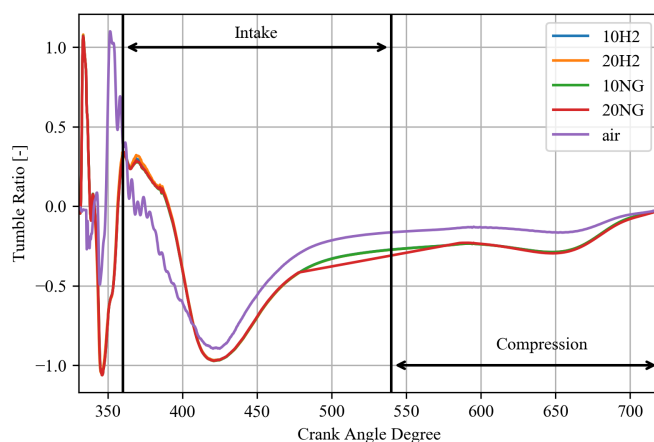


Figure 6.8: Tumble Ratio vs CAD for the difference substitution and enrichment levels.

As expected due the solutions of SR and TR shown in Fig. 6.7 and 6.8, respectively, CT ratio calculated values, presented in Fig. 6.9, have comparable results. Thus, the computation for CT rate of the 100 air case shows a smaller value than the results of the other cases except for the 20NG case. For CT rate, the value obtained from the simulation is similar to this obtained in the 100 air case. The values of the CT rate for 10-, 20H2 and 10NG cases are more greater than 20NG and 100 air cases. A comparable status was achieved in the end of the compression stroke (near 720 CAD) for the SR results shown in Fig. 6.7.

The velocity contour progression for the 100 air case is presented in the Fig. 6.10. The figure shows the results of the velocity contours along the intake and compression stroke (all the simulated range). High values of velocity are achieved in the first stage of the intake stroke (near 360 CAD) in the portion of valves overlap. It is important to note that in the valves overlap, a quantity of fuel is ejected outside via exhaust duct because the fluid pass directly from intake valve to exhaust valve and further to the exhaust duct. As the results presented in [44], the turbulence (instantaneous velocity variations) decays throw compression stroke. A wake below valve, specially intake valve (see Fig. 6.10 (e)), is perceived. In [35] is commented a similar result. They argue that a bigger valve diameter represents a better charge of the engine (more flow passing via intake valve) but

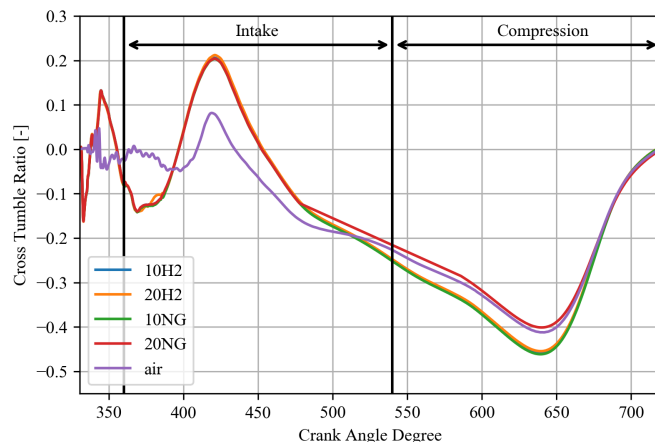


Figure 6.9: Cross Tumble Ratio vs CAD for the difference substitution and enrichment levels.

creates a blind zone below the valve where, in fact, there is no fluid. The pushing of the valve towards in the intake process forces the fluid to the bottom of the cylinder and, at the same time, a vacuum is created due to the piston motion. These situations sacrifice the zone below the intake valve where an absence of charge is encountered. Thus, there is the opportunity of a study focused in this phenomena in order to develop the best volumetric efficiency analyzing the called blind zone.

The diesel engines are engines of heterogeneous charge. Consequently, the turbulence has to be fixed near the point where the injection is made aiming to achieve the best mixing just after the SOI [8]. The TKE, in a common point where general diesel engines inject the liquid fuel (15 CAD bTDC in compression stroke [24, 50]), is presented in Fig. 6.11. Due to TKE contours configuration is recommendable to inject the diesel in the direction of the intake valve and the piston with the aim of taking advantage of the vortex energy. As shown in the figure, a concentrated TKE is computed just below of intake valve. This zone of high turbulence intensity is created by the piston motion and also for the IVC event. As reported in [32], intake stroke effects and changes affect directly how the fluid motion takes place in the compression stroke and, finally in TDC. Hence, the motion vortex created by the IVC event is kept until the final of the compression stroke. The air-fuel mixing could be improved if the fuel is injected in the direction where TKE presents the biggest values, due to the nature of variations in velocity achieved via turbulence.

Some velocity contours are presented in Fig. 6.12. The air-fuel mixture motion is perceived in the graph for all the simulated cases. The 20NG case presents a pronounced vortex below intake valve in the middle of the cylinder. This vortex is also seen in other cases included 100 air case. Another vortex takes place below exhaust valve. These vortex, apparently are formed

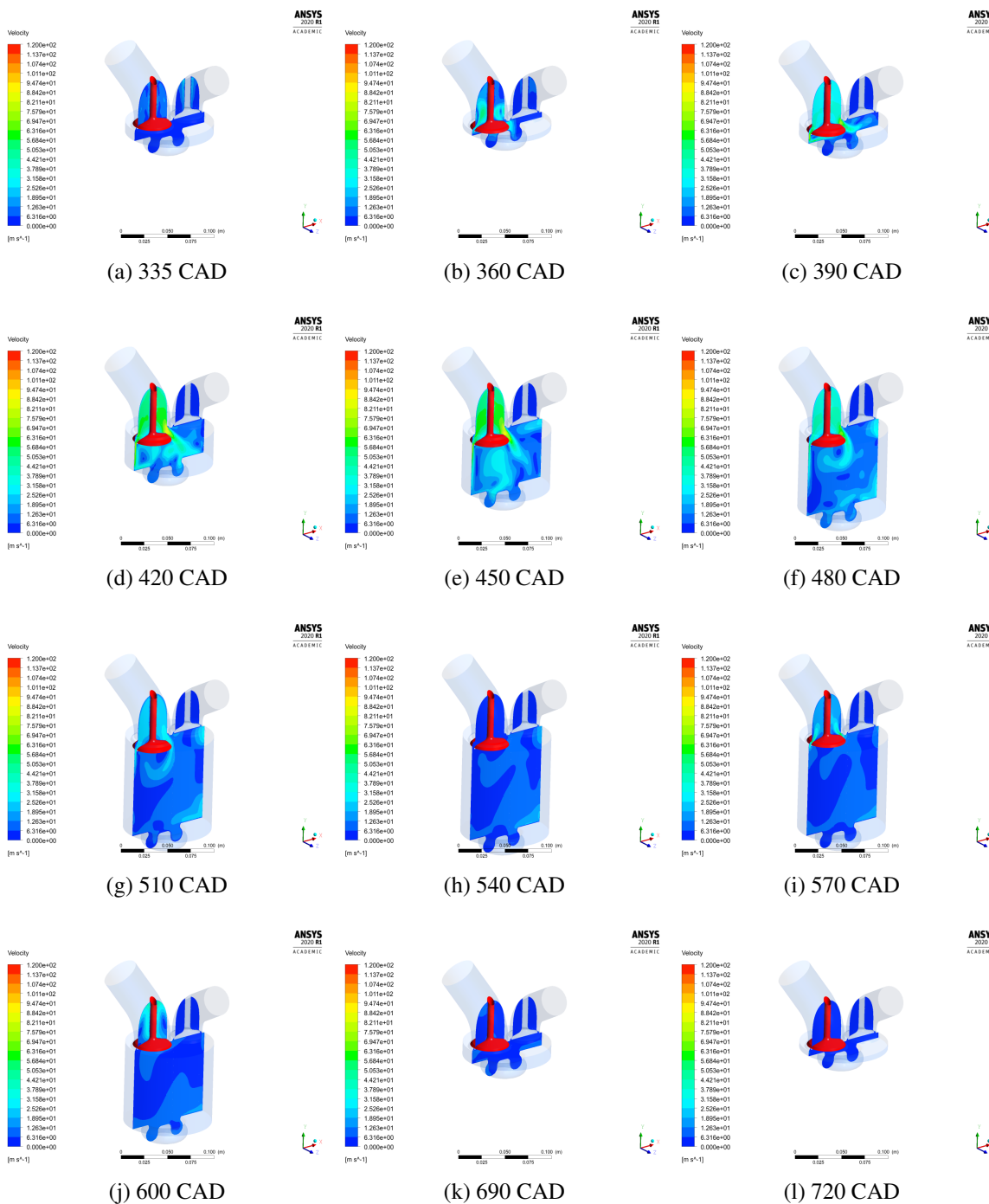


Figure 6.10: Velocity contours progression of the 100 air case.

because of the movement of the valves, creating vacuum dragging the fluid. In this portion of the compression stroke, the tumble ratio decreases and the vortex present are quenched because of the piston movement. As presented for the flow patterns (SR, TR and CT rate), the only air-fuel motion that reach TDC in the compression stroke with some value, is the swirl motion. That

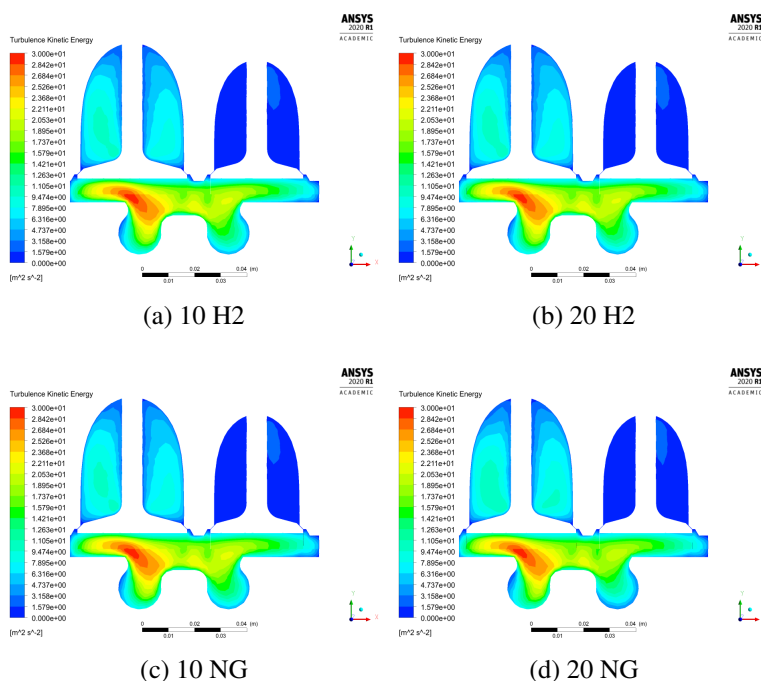


Figure 6.11: TKE prior to diesel injection for different cases of enrichment and substitution (705 CAD).

happens because of the movement nature of the swirl (around cylinder axis). As discussed above, the motion keeps its behavior until the final position in the TDC of the compression stroke.

Another important analysis can be made to the fuel distribution in the in-cylinder mixture. In [15] is concluded that an assumption of having uniform air-fuel mixture as inflow in the inlet for dual-fuel diesel engines is correct. The distribution in the intake valve is an homogeneous mixture of the species. They carried out a cold flow simulation where the primary fuel (NG or methanol in the mentioned study) was injected downstream of the intake valve, in the middle of the intake duct. As exposed, the results expose that it is completely correct an assumption of homogeneous mixture as inflow. In that way, the present simulation was initialized as a homogeneous mixture of species. In the Fig. 6.13 is presented the mass fraction distribution in combustion chamber of the primary fuel, in this case, hydrogen. As the initialization, there were no variations in the fuel concentration. The hydrogen is distributed homogeneously throughout the combustion chamber at TDC.

6.2.2 In-cylinder air motion

Some flow patterns can be appreciated in the Fig. 6.14. In the figure, 3D vectors are exposed in order to analyze the in-cylinder air flow motion. Some vortex are perceived in the figure. The

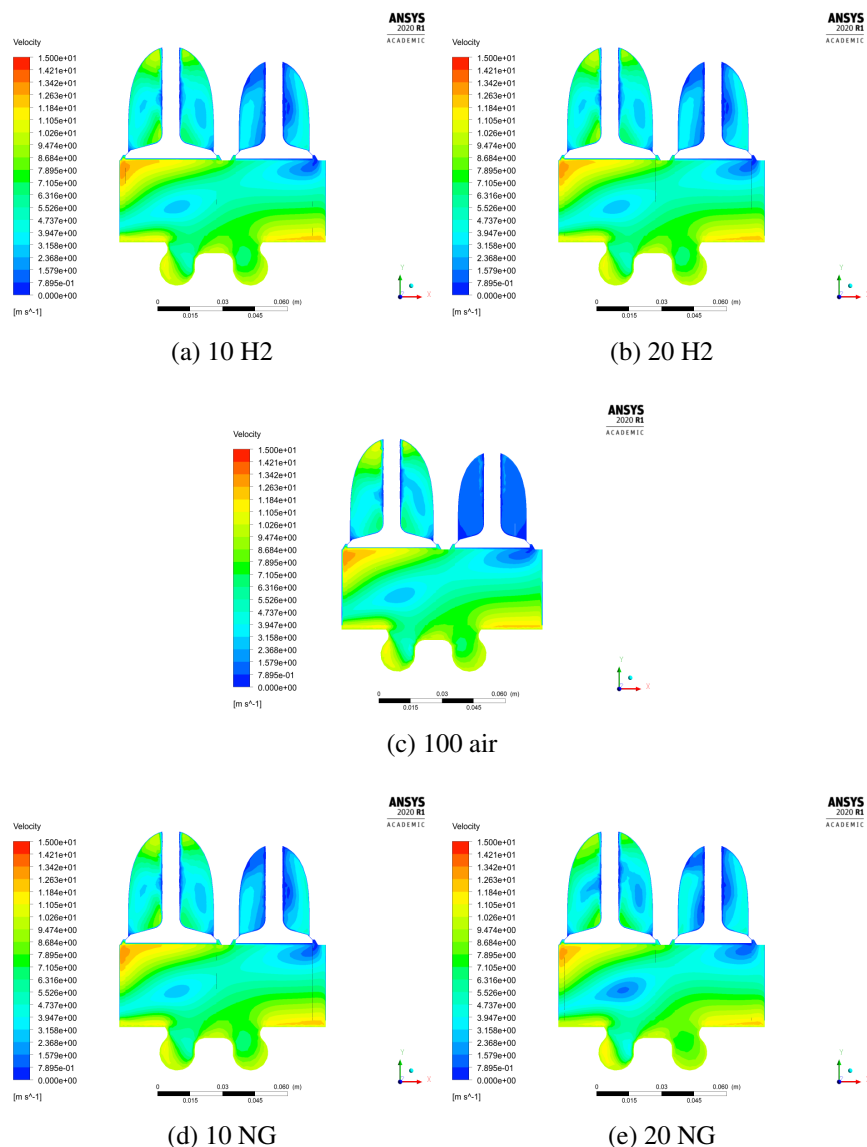


Figure 6.12: Velocity contours at 660 CAD for different cases of enrichment and substitution (705 CAD).

colored blue valve is the intake valve and the figure represents an intermediate stage of the intake stroke. It is possible to see the air-fuel motion entering cylinder around intake valve. If a detailed look is made over the figure, it is possible to see swirl, tumble the cross tumble patterns.

In an orthogonal plane to the cylinder is presented the mixture air-fuel vectors motion. These vectors can be seen in Fig. 6.15 and are established 15CAD bTDC in the compression stroke, in a expected point where the liquid fuel is injected. As expected from the results of Fig. 6.9, the slowest velocity appears for the 20NG case. The air-fuel motion is predominant just below intake valve. This result confirm the previous indicative that the fuel should be injected in that direction

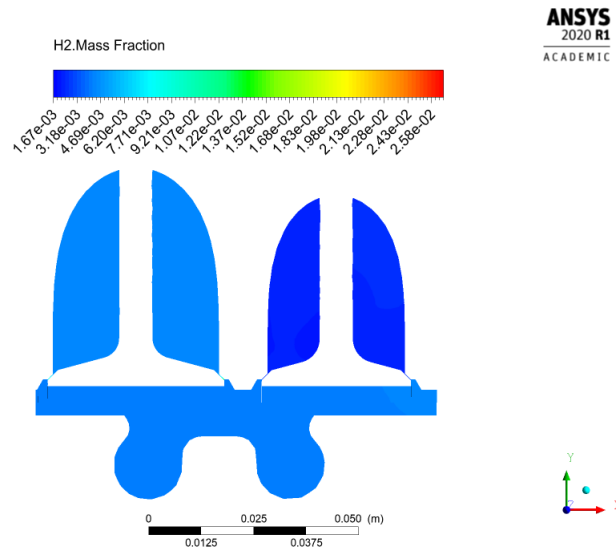


Figure 6.13: Hydrogen mass fraction of 10 H2 case at TDC after compression stroke.

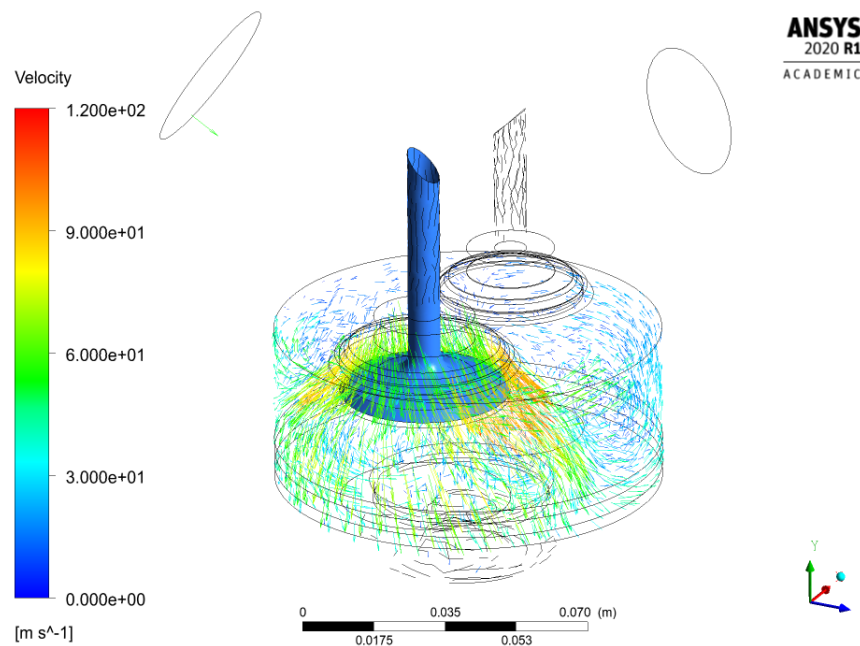


Figure 6.14: Velocity vectors in a 3D view in the middle stage of the intake stroke.

(aiming at the portion below intake valve) in order to take the biggest advantage from the turbulence and, consequently, having a better air-fuel mixing with the spray and a faster combustion. If the fuel is injected perpendicular to the cylinder head, the mixing of air-fuel with the liquid fuel will be poor, compared to the established idea of a different injection.

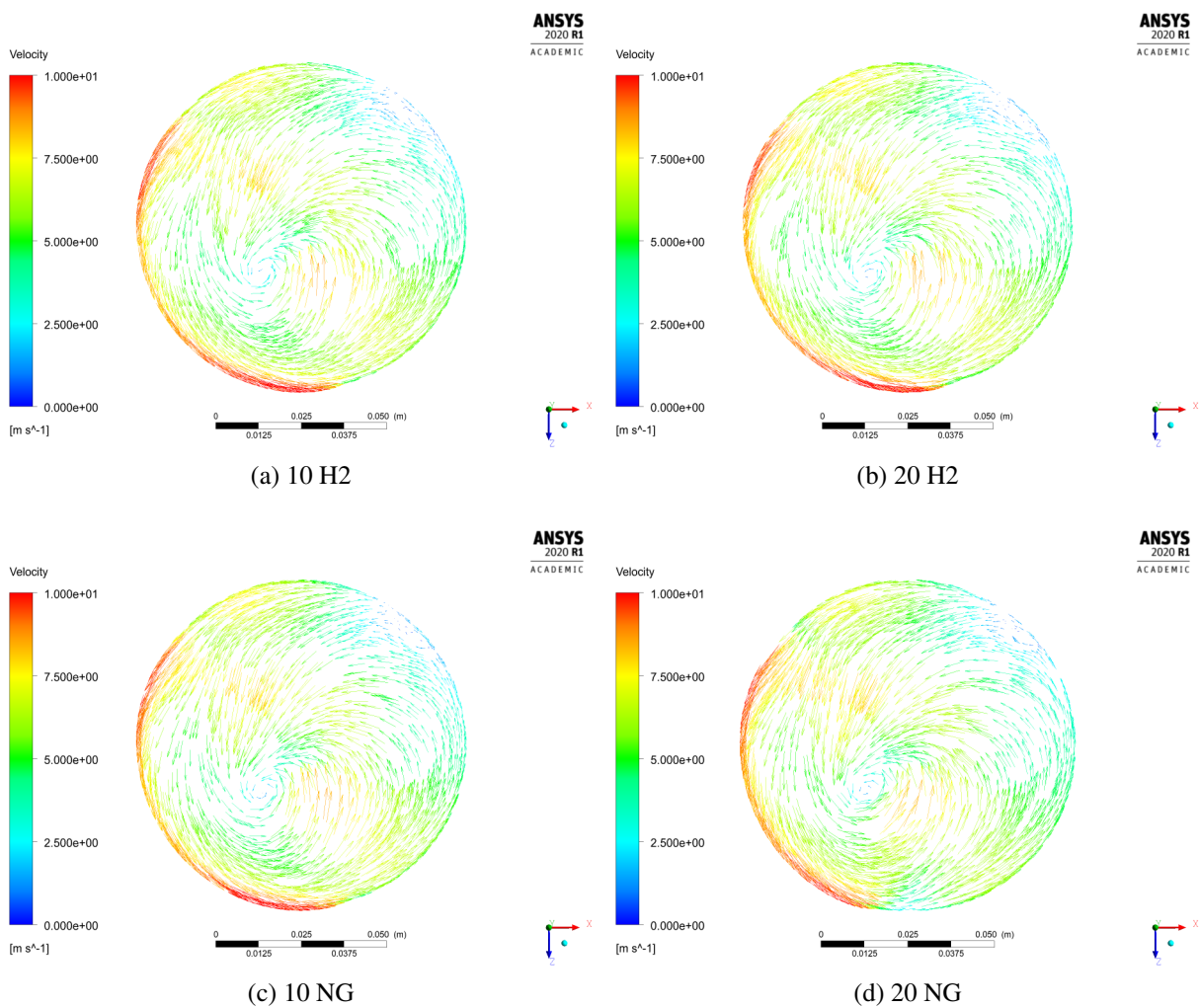


Figure 6.15: Flow patterns vectors perpendicular to the cylinder at 705 CAD (prior diesel injection) for different cases of enrichment and substitution.

Conclusions

1. Flow patterns and its behaviour (formation and motion) were captured with the model set.
2. As [1] concluded for marine engines with their work on CFD scavenging processes, the main conclusion of this project is an insight of a better flow field understanding in the diesel engine of the project. Subsequently, decisions can be taken based on the process comprehension. An important conclusion is the acquirement of the methodology to carry out this type of simulations. Engineering and scientific solutions can be studied in the future in a wide range of parameters.
3. If there are no experimental results, to validate the results a simple model (0D or 1D) is necessary in order to have a point of comparison.
4. The cold flow simulations are focused mainly on engineering aspects (increasing efficiencies, reducing thermal charges...), whereas for deeper fundamental aspects about understanding on fluid interactions, more complex simulations have to be made (LES or DNS).
5. For cold flow simulations, it is better to use Spalart-Allmaras turbulence model, because of its reduced computational time and good accuracy compared with Standard $k - \epsilon$.
6. A speculated trend was found for the effect of enrichment and substitution levels over the flow patterns, observing an increasing in the magnitude of the computed values for SR, TR and Cross TR when the levels are increased. More simulations are needed to establish the trend (or refuse it).

Bibliography

- [1] F. H. Andersen, J. Hult, K.-J. Nogenmyr, and S. Mayer. Cfd analysis of the scavenging process in marine two-stroke diesel engines. In *Internal Combustion Engine Division Fall Technical Conference*, volume 46162, page V001T01A002. American Society of Mechanical Engineers, 2014.
- [2] J. Anderson. Computational fluid dynamics : the basics with applications. In -, 1995.
- [3] I. ANSYS. *Internal Combustion Engines in Workbench*. ANSYS, Inc., 2013.
- [4] I. ANSYS. Ansys fluent theory guide. *ANSYS Inc., USA. Release*, 15.0:724–746, 2013.
- [5] D. Apsley and M. Leschziner. Advanced turbulence modelling of separated flow in a diffuser. *Flow, turbulence and combustion*, 63(1):81–112, 2000.
- [6] G. Arce. Plan de acción indicativo de eficiencia energética 2017-2022. *Una Realidad y Oportunidad para Colombia. Ministerio de Minas y Energía. Unidad de Planeación Minero Energética UPME*, 2017.
- [7] A. Azad, P. Halder, K. Nanthagopal, and B. Ashok. Investigation of diesel engine in cylinder flow phenomena using cfd cold flow simulation. In *Advanced Biofuels*, pages 329–336. Elsevier, 2019.
- [8] S. Bari and I. Saad. Cfd modelling of the effect of guide vane swirl and tumble device to generate better in-cylinder air flow in a ci engine fuelled by biodiesel. *Computers & Fluids*, 84:262–269, 2013.
- [9] I. D. Bedoya, A. A. Arrieta, and F. J. Cadavid. Effects of mixing system and pilot fuel quality on diesel–biogas dual fuel engine performance. *Bioresource technology*, 100(24):6624–6629, 2009.
- [10] J. Benajes, S. Molina, J. Garcia, and J. Riesco. The effect of swirl on combustion and exhaust emissions in heavy-duty diesel engines. *Proceedings of the Institution of Mechanical Engineers, Part D: Journal of Automobile Engineering*, 218(10):1141–1148, 2004.

-
- [11] E. Blayo and L. Debreu. Revisiting open boundary conditions from the point of view of characteristic variables. *Ocean modelling*, 9(3):231–252, 2005.
- [12] A. Boretti. The future of the internal combustion engine after “diesel-gate”. Technical report, SAE Technical Paper, 2017.
- [13] F. Brandl, I. Reverencic, W. Cartellieri, and J. Dent. Turbulent air flow in the combustion bowl of a di diesel engine and its effect on engine performance. *SAE Transactions*, pages 172–199, 1979.
- [14] K. Cacua, A. Amell, and F. Cadavid. Effects of oxygen enriched air on the operation and performance of a diesel-biogas dual fuel engine. *Biomass and bioenergy*, 45:159–167, 2012.
- [15] G. Decan, B. De Buyzerie, T. Lucchini, G. D’Errico, and S. Verhelst. Cold flow simulation of a dual-fuel engine for diesel-natural gas and diesel-methanol fuelling conditions. Technical report, SAE Technical Paper, 2021.
- [16] C. del motor. Pistones-camisas-equipos. Technical report, -, 2019. URL <https://www.comercialdelmotor.com/pdf/catalogo-pistones.pdf>.
- [17] B. Engquist and A. Majda. Absorbing boundary conditions for numerical simulation of waves. *Proceedings of the National Academy of Sciences*, 74(5):1765–1766, 1977.
- [18] C. J. Freitas. The issue of numerical uncertainty. *Applied Mathematical Modelling*, 26(2): 237–248, 2002.
- [19] M. Gül, M. Yılmaz, S. Nas, and M. Yıldırım. In-cylinder cold flow modeling with spray interaction in heavy duty di-ci engine. *ICAT08*, 13:14, 2008.
- [20] N. Hasan, J. Adeba, A. Bulcha, and A. Samad. Computational fluid dynamic parametric investigation of cold flow simulation for internal combustion engine. In *AIP Conference Proceedings*, volume 2134, page 030004. AIP Publishing LLC, 2019.
- [21] S. Heredia Quintana. Desarrollo e implementación de una metodología secuencial cfd-cinética química detallada para el análisis de la combustión hcci y sus principales emisiones en motores estacionarios. *Repositorio UdeA*, 2020.
- [22] J. B. Heywood. *Internal combustion engine fundamentals*. McGraw-Hill Education, 2018.
- [23] P. Hill and D. Zhang. The effects of swirl and tumble on combustion in spark-ignition engines. *Progress in energy and combustion science*, 20(5):373–429, 1994.
-

-
- [24] A. Jamil, M. B. Baharom, and A. R. A. Aziz. Ic engine in-cylinder cold-flow analysis—a critical review. *Alexandria Engineering Journal*, 60(3):2921–2945, 2021.
- [25] T. V. Johnson. Review of diesel emissions and control. *International Journal of Engine Research*, 10(5):275–285, 2009.
- [26] T. V. Johnson. Diesel emissions in review. *SAE International Journal of Engines*, 4(1):143–157, 2011.
- [27] M. KAPLAN. Influence of swirl, tumble and squish flows on combustion characteristics and emissions in internal combustion engine-review. *International Journal of Automotive Engineering and Technologies*, 8(2):83–102, 2019.
- [28] Y. Karagöz, T. Sandalcı, L. Yüksek, A. S. Dalkılıç, and S. Wongwises. Effect of hydrogen–diesel dual-fuel usage on performance, emissions and diesel combustion in diesel engines. *Advances in Mechanical Engineering*, 8(8):1687814016664458, 2016.
- [29] G. A. Karim. The dual fuel engine of the compression ignition type-prospects, problems and solutions-a review. *SAE transactions*, pages 569–577, 1983.
- [30] R. Kavtaradze, T. Natriashvili, and S. Gladyshev. Hydrogen-diesel engine: Problems and prospects of improving the working process. Technical report, SAE Technical Paper, 2019.
- [31] W. H. Kurniawan, S. Abdullah, and A. Shamsudeen. A computational fluid dynamics study of cold-flow analysis for mixture preparation in a motored four-stroke direct injection engine. *Journal of applied Sciences*, 7(19):2710–2724, 2007.
- [32] T.-M. Liou and D. Santavicca. Cycle resolved turbulence measurements in a ported engine with and without swirl. *SAE transactions*, pages 131–144, 1983.
- [33] A. C. Lloyd and T. A. Cackette. Diesel engines: environmental impact and control. *Journal of the Air & Waste Management Association*, 51(6):809–847, 2001.
- [34] T. Lucchini, G. D’Errico, H. Jasak, and Z. Tukovic. Automatic mesh motion with topological changes for engine simulation. Technical report, SAE Technical Paper, 2007.
- [35] G. Martinas, O. Cupsa, L. Stan, and A. Arsenie. Cold flow simulation of an internal combustion engine with vertical valves using layering approach. In *IOP Conference Series: Materials Science and Engineering*, volume 95, page 012043. IOP Publishing, 2015.
-

-
- [36] A. Mena, M. Lounici, F. Amrouche, K. Loubar, and M. Kessal. Cfd analysis of hydrogen injection pressure and valve profile law effects on backfire and pre-ignition phenomena in hydrogen-diesel dual fuel engine. *International Journal of Hydrogen Energy*, 44(18):9408–9422, 2019.
- [37] F. Menter. Zonal two equation kw turbulence models for aerodynamic flows. In *23rd fluid dynamics, plasmadynamics, and lasers conference*, page 2906, 1993.
- [38] F. R. Menter. Two-equation eddy-viscosity turbulence models for engineering applications. *AIAA journal*, 32(8):1598–1605, 1994.
- [39] W. L. Oberkampf and T. G. Trucano. Verification and validation in computational fluid dynamics. *Progress in aerospace sciences*, 38(3):209–272, 2002.
- [40] F. Payri, J. Benajes, X. Margot, and A. Gil. Cfd modeling of the in-cylinder flow in direct-injection diesel engines. *Computers & fluids*, 33(8):995–1021, 2004.
- [41] Y. Qi, L. Dong, H. Liu, P. Puzinauskas, and K. Midkiff. Optimization of intake port design for si engine. *International Journal of Automotive Technology*, 13(6):861–872, 2012.
- [42] S. H. Quintana and A. D. Morales-Rojas. Desarrollo y validación de un modelo cero dimensional de dos zonas para el análisis de la combustión en motores de encendido provocado. *Revista CINTEX*, 23(2):25–33, 2018.
- [43] G. Regner, D. Johnson, J. Koszewnik, E. Dion, F. Redon, and L. Fromm. Modernizing the opposed piston, two stroke engine for clean, efficient transportation. Technical report, SAE Technical Paper, 2013.
- [44] N. M. Shafie and M. M. Said. Cold flow analysis on internal combustion engine with different piston bowl configurations. *Journal of Engineering Science and Technology*, 12(4):1048–1066, 2017.
- [45] V. Smil. The two prime movers of globalization: history and impact of diesel engines and gas turbines. *Journal of Global History*, 2(3):373, 2007.
- [46] P. Spalart and S. Allmaras. A one-equation turbulence model for aerodynamic flows. In *30th aerospace sciences meeting and exhibit*, page 439, 1992.
- [47] A. Torregrosa, P. Olmeda, B. Degraeuwe, and M. Reyes. A concise wall temperature model for di diesel engines. *Applied Thermal Engineering*, 26(11-12):1320–1327, 2006.
-

-
- [48] T. Urushihara, T. Murayama, Y. Takagi, and K.-H. Lee. Turbulence and cycle-by-cycle variation of mean velocity generated by swirl and tumble flow and their effects on combustion. *SAE transactions*, pages 1382–1389, 1995.
- [49] H. K. Versteeg and W. Malalasekera. *An introduction to computational fluid dynamics: the finite volume method*. Pearson education, 2007.
- [50] K. Wannatong, N. Akarapanyavit, S. Siengsanorh, and S. Chanchaona. Combustion and knock characteristics of natural gas diesel dual fuel engine. Technical report, SAE Technical Paper, 2007.
- [51] S. Wei, F. Wang, X. Leng, X. Liu, and K. Ji. Numerical analysis on the effect of swirl ratios on swirl chamber combustion system of di diesel engines. *Energy Conversion and Management*, 75:184–190, 2013.
- [52] X. Yang, S. Gupta, T.-W. Kuo, and V. Gopalakrishnan. Rans and large eddy simulation of internal combustion engine flows—a comparative study. *Journal of Engineering for Gas Turbines and Power*, 136(5), 2014.
- [53] K. Zaker, M. H. Askari, A. Jazayeri, R. Ebrahimi, B. Zaker, and M. Ashjaee. Open cycle cfd investigation of si engine fueled with hydrogen/methane blends using detailed kinetic mechanism. *International Journal of Hydrogen Energy*, 40(40):14006–14019, 2015.
-